To the Graduate Council:

I am submitting herewith a thesis written by Edward T. Karkut entitled "Use of a Gaussian Transducer to Correct Ultrasonic Wave Attenuation for Diffraction and Wedge Angle in Solids." I have examined the final copy of this thesis for form and content and recommend that it be accepted in partial fulfillment of the requirements for the degree of Master of Science, with a major in Engineering Science and Mechanics.

M. A. Breazeale

M. A. Breazeale, Major Professor

We have read this thesis and recommend its acceptance:

Jerry E. Stoneking

Walter F. Jones

Accepted for the Council:

C. W. Minkel

Vice Provost
and Dean of the Graduate School

STATEMENT OF PERMISSION TO USE

In presenting this thesis in partial fulfillment of the requirements for a Master's degree at The University of Tennessee, Knoxville, I agree that the Library shall make it available to borrowers under rules of the Library. Brief quotations from this thesis are allowable without special permission, provided that accurate acknowledgment of source is made.

Permission for extensive quotation from or reproduction of this thesis may be granted by my major professor, or in his absence, by the Head of Interlibrary Services when, in the opinion of either, the proposed use of the material is for scholarly purposes. Any copying or use of the material in this thesis for financial gain shall not be allowed without my written permission.

Signature B Korkut

Date 29 June '85

USE OF A GAUSSIAN TRANSDUCER TO CORRECT ULTRASONIC WAVE ATTENUATION FOR DIFFRACTION AND WEDGE ANGLE IN SOLIDS

A Thesis

Presented for the

Master of Science

Degree

The University of Tennessee, Knoxville

Edward T. Karkut

August 1985

ACKNOWLEDGMENTS

The author wishes to express his appreciation to the following individuals and agencies without whose support this investigation would not have been possible:

Dr. M. A. Breazeale for his helpful suggestions and advice during the experimental portion of this study and the writing of this thesis;

Professor G. Du for providing much of the theoretical background for this investigation and suggestions regarding the experimental techniques;

Canadian Armed Forces for providing the author with the opportunity to participate in the Graduate Training Program;

UT-ORNL Science Alliance Program for providing the funds to procure the steel sample used in this study;

Canadian Forces Aerospace Maintenance Development Unit and Oak Ridge National Laboratory for manufacturing the samples used in this study;

United States Office of Naval Research for providing the author with the use of laboratory equipment at The University of Tennessee; and

Mrs. Maxine Martin for typing this manuscript and making many useful suggestions during the course of the writing.

Finally, the author would like to express his gratefulness to his wife Kathy whose love, support and encouragement were the contributing factors to the timely completion of this thesis.

ABSTRACT

A study is made of ultrasonic waves propagating in steel samples whose surfaces are intentionally nonparallel. By using a recently designed Gaussian transducer one now is able to correct for the effects of both diffraction and wedge angle on measured pressure amplitudes and hence determine the intrinsic attenuation of the material under investigation. A through-transmission technique is used to obtain pulse echo patterns from a steel plate having facets whose angles range between 0 and 0.018 radians. A mathematical model is developed which corrects ultrasonic echo heights for diffraction and wedge angle.

Finally, a computer program is given and its use to correct ultrasonic echo amplitudes for frequencies of 3 and 6 MHz is illustrated.

TABLE OF CONTENTS

LIST OF FIGURES

CHAPTER I

INTRODUCTION

For many years, the attenuation of pulsed ultrasonic waves in structural materials has been investigated as a means to determine material properties. Strong empirical correlations between energy losses of ultrasonic waves and material variations due to hardening, annealing, quenching and cold working in laboratory samples have evolved from several studies (Roderick and Truell, 1952; Rogers, 1965; Papadakis, 1970). As this ultrasonic technique is more universally accepted and added to conventional material evaluation methods, however, it becomes even more important that research be conducted on the factors that affect its accuracy and precision.

One such factor commonly encountered in practical nondestructive testing (NDT) situations is losses resulting from nonparallelism between sample faces (wedge loss). In calculating intrinsic attenuation, investigators have observed that appreciable errors can result if wedge loss is not correctly accounted for. But in attempting to account for wedge loss one encounters the fact that a transducer produces a complicated diffraction field whose effects are superimposed on wedge loss and intrinsic attenuation and that the diffraction field is especially complicated in the nearfield where most contact NDT measurements are made. In an attempt to simplify the analysis, investigators have made the expedient assumption that nonparallelism and diffraction produce separate effects on the ultrasonic waves and therefore can be calculated separately. Although it is expedient, this assumption is incorrect. In this thesis it is observed that losses due to diffraction and nonparallelism are not independent and therefore must be corrected for simultaneously.

A review of the literature on the diffraction problem shows that the majority of researchers have focused their attention on the form of the diffraction integral given in 1878 by Lord Rayleigh (1945) and its solution for a piston radiator. The first solution of this integral was published by Lommel (1885) who applied it to the propagation of light by utilizing the Kirchhoff approximation. Since this solution was found difficult to use; viz., it was in the form of an infinite sum of Bessel functions, Huntington et al. (1948) published a table of diffraction corrections based on numerical integration of Lommel's results. Inasmuch as the relationship that Huntington et al. used was an approximation, the diffraction corrections that they obtained in the vicinity of the radiator were found to diverge. This restricted the application of their results to only those NDT situations in which the propagation path was sufficiently great (usually the immersion technique). Later Seki, Granato, and Truell (1956) recalculated the Lommel diffraction correction at closer intervals than Huntington et al. by performing the required integrations graphically.

Rogers and Van Buren (1974) obtained an analytical solution for the Lommel diffraction correction integral which was valid at all distances. This solution was applicable to the transmission of sound between two discs of the same size and parallel to each other and allowed them to plot the complete diffraction correction curve for all distances between the transducers. Although Rogers and Van Buren's solution of the Lommel diffraction correction integral resolved the diffraction correction problem of a piston transducer, its application in the present study is limited since it assumes parallelism between the source and receiving transducer. Most of our measurements are made in samples whose faces are intentionally nonparallel.

In the early diffraction studies the surface of the sample under investigation were conveniently assumed to be parallel. However, this assumption is not valid in many NDT situations and large errors may result in attenuation measurements if parallelism is assumed in the theoretical analysis when it is not realized in the experiment. This fact was realized by Vary (1980). In his review of attenuation measurement he cautioned that ultrasonic waves should be transmitted between parallel surfaces to avoid problems with beam divergence (diffraction) and geometrical effects. But this advice cannot always be heeded.

The problem of mathematically correcting for nonparallelism was initially investigated by Truell and Oats (1963). Their model, based upon phase cancellation of infinite plane waves, indicated that the diffraction pattern in a wedged sample was modulated by a function $2\ J_1(Ka \sin \gamma n)/Ka \sin \gamma n$. Further, they observed that their model corrected the experimental echo pattern at a frequency of 85 MHz better than at 30 MHz. They did not present any data for frequencies as low as 1 to 5 MHz, the frequencies most commonly used in NDT. A subsequent investigation by Calder (1978) modified the Truell and Oates model by correcting for anisotropy in the sample. He applied this correction to a wedged sample and to a hemispherical reflector. In his study he found that at a frequency of 5 MHz he was able to correct the echo train produced by the hemispherical reflector; however, he was unable to adjust echoes observed in the presence of a nonparallel reflector.

The problem of nonparallelism was re-examined at the frequency range between 3 to 9 MHz by Boudreault (1982). In his study Boudreault modified the Truell and Oates model by removing the plane wave approximation and considering the diffraction field of a piston transducer by defining the pressure in the sound field through the use of a unique coordinate transformation. The geometrical correction as defined in his study was found correctly to adjust the first four echoes for frequencies between 3 and 6 MHz and wedge angles less than 4×10^{-3} radians (0.23°).

In a sense the present study is an extension of that of Boudreault (1982). In the present study we make use of the mathematical simplification afforded by use of a transducer whose amplitude distribution is described by a Gaussian function. The losses resulting from nonparallelism and diffraction are corrected for simultaneously. This requires that we determine the pressure at a point in the diffraction field of a Gaussian radiator and integrate this pressure over a receiving crystal in order to get its response. In the integration we use the coordinate transformation of Boudreault and take into account the variation of phase felt by the receiving crystal with successive reflection from a wedged sample surface. The result is a correction which may be applied to adjust attenuation measurements in the usual NDT frequency range as long as Gaussian transducers are used.

The first attempt to produce a Gaussian transducer was made by Von Haselberg and Krautkrämer (1959) by depositing a rosette-shaped electrode on a transducer. A focused field produced by the transducer was studied by Filipcznski and Etienne (1973). Zerwekh and Claus (1981) used a ring electrode configuration and a resistor chain to adjust the amplitude to produce a piecewise continuous Gaussian distribution. Martin and Breazeale (1971) and Breazeale et al. (1981) described a means by which a one-dimensional Gaussian distribution could be produced by using electrical fringing. Du and Breazeale (1984) gave an analytical expression which describes the radiation field of a radially symmetric Gaussian amplitude distribution and designed a practical transducer. Both the mathematical simplification in the evaluation of the diffraction integral brought about by use of the Gaussian function and the attractive features of the Gaussian transducer (absence of pressure maxima and minima near the transducer) as pointed out by the Du and Breazeale study suggested the possibility of its use to facilitate calculation of geometrical losses resulting from diffraction in a wedged sample. The results of this investigation are reported in this thesis.

CHAPTER II

THEORETICAL ANALYSIS

A. Wave Propagation Theory

1. Ultrasonic Attenuation

a. Definition of the attenuation coefficient. Media in which ultrasonic waves propagate are lossy and consequently the amplitude of these waves decreases with distance. Considering plane waves (where there is no geometrical beam spread), one may write the following expression for the pressure amplitude after travelling a distance Δx:

$$p(x,t) = p_0 \, e^{i(\omega t - k\Delta x)} , \qquad (2\text{-}1)$$

where ω is the angular frequency and $k = \frac{2\pi}{\lambda}$ is the propagation constant.

An expression for an attenuated wave may be found directly from Equation (2-1) by assuming that the propagation constant is complex. Taking

$$k = k_1 - i\alpha , \qquad (2\text{-}2)$$

one obtains the equation of the attenuated plane wave to be:

$$p(x,t) = [e^{-\alpha\Delta x}] p_0 \, e^{i(\omega t - k_1 \Delta x)} . \qquad (2\text{-}3)$$

The modulus of Equation (2-3) is found to be:

$$p_{max} = p_0 \, e^{-\alpha \Delta x} \quad . \tag{2-4}$$

From Equation (2-4) one obtains an expression for the attenuation coefficient in the form:

$$\alpha = \frac{20}{\Delta x} \log_{10} \left(\frac{p_0}{p_{max}(x)} \right) \quad , \tag{2-5}$$

where α is expressed in db per unit of length. This expression is used throughout this thesis.

b. Attenuation correction. The exact determination of the intrinsic attenuation of a material as described by Equation (2-5) often requires correction for effects ignored in writing the equation. For example, it has been found that geometrical losses resulting from diffraction, as well as phase cancellation from nonparallelism of the receiver and transmitter, both affect the observed echo pattern and therefore the attenuation measurement.

As we are attempting precisely to measure only those losses contributed by the material properties, the geometrical losses must be properly accounted for in our study. This is done by correcting the measured pressure values for geometrical effects and using the corrected pressure in Equation (2-5). The means to correct for the effect of geometrical losses on the measured decay pattern is the subject of the next section.

2. Diffraction Theory

a. Assumption and basic formulae. The propagation of an ultrasonic wave in a fluid is governed by the wave equation, which is derived from three basic equations in physics, the equation of continuity:

$$\frac{d\rho}{dt} + \nabla \cdot (\rho\overline{u}) = 0 , \qquad (2\text{-}6)$$

Navier-Stokes equation:

$$\rho \frac{d\overline{u}}{dt} = - \nabla_p + \left(\frac{4}{3}\mu + K\right)\nabla^2\overline{u},\ \nabla x\overline{u} = 0 , \qquad (2\text{-}7)$$

and the equation of state (Aanonsen et al., 1984):

$$\nabla_p = c^2\nabla_\rho - \left(k\left(\frac{\gamma - 1}{\gamma}\right) + R\right)\rho\nabla^2\overline{u} . \qquad (2\text{-}8)$$

Here are $d/dt = \partial/\partial t + \overline{u} \cdot \nabla$, $\overline{u}$ velocity, p pressure, ρ density, c speed of sound; μ, K, k and R are, respectively, the coefficients of shear and bulk viscosity, thermal conductivity and relaxation and $\gamma = C_p/C_v$ is the ratio between specific heat at constant pressure and constant volume.

The general expression of the wave equation is obtained from the above equations in the case of a narrow, progressive sound beam by utilizing the parabolic approximation which in effect requires $ka \gg 1$. A nondimensional form of the resulting nonlinear wave equation (the parabolic equation) is given by (Aanonsen et al., 1984):

$$\left(4\,\frac{\partial^2}{\partial\tau\partial\sigma} - \overline{\nabla}_1^{\,2} - 4\alpha r_0\,\frac{\partial^3}{\partial\tau^3}\right)\overline{p} = \frac{2r_0}{\ell_D}\,\frac{\partial^2}{\partial\tau^2}\,\overline{p}^2 \ , \qquad (2\text{-}9)$$

where $\sigma = \frac{z}{r_0}$, $r_0 = \frac{a^2\omega}{2c_0}$, $\tau = \omega(t - \frac{z}{c_0})$, $\overline{p} = \rho/\rho_0 c_0 u_0$, $\ell_D = \frac{c_0 T}{B\varepsilon}$, $\alpha = \frac{D}{2c_0^{\,3}T^2}$, $D = \frac{4}{3}\,\frac{\mu + {}^0k}{\rho} + \frac{\gamma - 1}{\gamma}\,K + R$ and $\nabla_1^{\,2}$ is the nondimensional form of the Laplace operator, viz., $\nabla_1^{\,2} = \frac{1}{\varepsilon}\,\frac{\partial}{\partial\varepsilon}\,(\varepsilon\,\frac{\partial}{\partial\varepsilon})$, where $\varepsilon = \rho/a$ and ρ is the radial coordinate.

Neglecting the nonlinear terms of Equation (2-9), one may obtain the following linear equation:

$$\left(4\,\frac{\partial^2}{\partial\tau\partial\sigma} - \overline{\nabla}_1^{\,2} - 4\alpha r_0\,\frac{\partial^3}{\partial\tau^3}\right)\overline{p} = 0 \ .$$

Now, by seeking a solution of this equation in the form $\overline{p} = \exp(-i\tau)\overline{p}_1(\sigma)$, one gets an equation for the complex amplitude $\overline{p}_1$:

$$\left(-\,4i\,\frac{\partial}{\partial\sigma} - 4\alpha r_0 i - \overline{\nabla}_1^{\,2}\right)\overline{p}_1 = 0 \ . \qquad (2\text{-}10)$$

To solve Equation (2-10), one introduces the Hankel transformation

$$\overline{p}_1(\varepsilon,\sigma) = \int_0^\infty J_0(\varepsilon s)\tilde{p}_1(s,\sigma)s\,ds \ , \qquad (2\text{-}11a)$$

and its inverse

$$\tilde{p}_1(s,\sigma) = \int_0^\infty \overline{p}_1(\varepsilon',\sigma)J_0(\varepsilon' s)\varepsilon' d\varepsilon' \ . \qquad (2\text{-}11b)$$

Substituting Equation (2-11a) into Equation (2-10), one gets:

$$- 4i \int_0^\infty J_0(\varepsilon s)sds \frac{d}{d\sigma} \tilde{p}_1(s,\sigma) - 4i\alpha r_0 \int_0^\infty \tilde{p}_1(s,\sigma)J_0(\varepsilon s)sds$$

$$- \int_0^\infty \tilde{p}_1(s,\sigma)sds\overline{\nabla}_1{}^2 J_0(\varepsilon s) = 0 \ ,$$

or

$$- 4i \int_0^\infty J_0(\varepsilon s)sds \frac{d}{d\sigma} \tilde{p}_1(s,\sigma) - 4i\alpha r_0 \int_0^\infty \tilde{p}_1(s,\sigma)J_0(\varepsilon s)sds$$

$$- \int_0^\infty \tilde{p}_1(s,\sigma)sds[\overline{\nabla}_1{}^2 J_0(\varepsilon s) + s^2 J_0(\varepsilon s) - s^2 J_0(\varepsilon s)] = 0 \ . \tag{2-12}$$

From Watson (1944):

$$\overline{\nabla}_1{}^2 J_0(\varepsilon s) + s^2 J_0(\varepsilon s) = 0 \ .$$

Thus Equation (2-12) becomes:

$$- 4i \int_0^\infty J_0(\varepsilon s)sds \frac{d}{d\sigma} \tilde{p}_1(s,\sigma) - 4i\alpha r_0 \int_0^\infty \tilde{p}_1(s,\sigma)J_0(\varepsilon s)sds$$

$$+ \int_0^\infty \tilde{p}_1(s,\sigma)sds \ s^2 J_0(\varepsilon s) = 0 \ . \tag{2-13}$$

From Equation (2-13) one finds that the inverse Hankel transform of the pressure satisfies the ordinary differential equation

$$\frac{d\tilde{p}_1(s,\sigma)}{\tilde{p}_1(s,\sigma)} = \left(-\alpha r_0 - \frac{is^2}{4}\right) d\sigma \quad ,$$

which has the solution

$$\tilde{p}_1(s,\sigma) = \tilde{p}_1(\varepsilon,0)e^{(-\alpha r_0 - \frac{is^2}{4})\sigma} \quad . \tag{2-14}$$

Now if, initially at $\sigma = 0$,

$$\overline{p}_1(\varepsilon',0) = f(\varepsilon') \ ,$$

then, at $\sigma = 0$, the inverse Hankel transform becomes

$$\tilde{p}_1(s,0) = \int_0^\infty f(\varepsilon')J_0(\varepsilon' s)\varepsilon' d\varepsilon' \ .$$

Thus, by forming $\overline{p}_1$ by means of the Hankel transformation one gets:

$$\overline{p}_1(\varepsilon,\sigma) \doteq \int_0^\infty f(\varepsilon')\varepsilon' d\varepsilon' \int_0^\infty J_0(\varepsilon' s)J_0(\varepsilon s)e^{(-\alpha r_0 - \frac{is^2}{4})\sigma} sds \ . \tag{2-15}$$

From Watson (1944):

$$\int_0^\infty e^{-pt^2} J_0(at)J_0(bt)tdt = \frac{1}{2p^2} e^{-\frac{a^2+b^2}{4p^2}} J_0\left(\frac{ab}{2p^2}\right) \ .$$

Thus, Equation (2-15) becomes

$$\overline{p}_1(\varepsilon,\sigma) = \int_0^\infty e^{-\alpha r_0 \sigma} - \frac{2i}{\sigma} \exp\left(i \ \frac{\varepsilon'^2 + \varepsilon^2}{\sigma}\right) J_0(\frac{2\varepsilon\varepsilon'}{\sigma}) f(\varepsilon')\varepsilon' d\varepsilon' \ . \tag{2-16}$$

Finally, rewriting Equation (2-16) one gets as the linearized solution of the parabolic equation:

$$\overline{p}_1(\varepsilon,\sigma,\tau) = \mathrm{Re}[if_1(\varepsilon,\sigma)\exp(-i\tau - \alpha r_0\sigma)] \ , \tag{2-17}$$

where

$$f_1(\varepsilon,\sigma) = \frac{2}{i\sigma}\int_0^\infty \exp\left(i\ \frac{\varepsilon'^2 + \varepsilon^2}{\sigma}\right) J_0\left(\frac{2\varepsilon\varepsilon'}{\sigma}\right) f(\varepsilon')\varepsilon' d\varepsilon' \ . \tag{2-17a}$$

Now, let us consider the situation in which the initial disturbance on the boundary takes the form of a Gaussian function

$$f(\varepsilon') = \left(e^{-B\varepsilon'^2}\right) ,$$

where B is defined as the Gaussian coefficient. Equation (2-17a) then becomes

$$f_1(\varepsilon,\sigma) = \frac{2}{i\sigma}\int_0^\infty J_0\left(\frac{2\varepsilon\varepsilon'}{\sigma}\right)\exp\left(\left(\frac{i}{\sigma} - B\right)\varepsilon'^2 + \frac{i\varepsilon^2}{\sigma}\right)\varepsilon' d\varepsilon' \ . \tag{2-18}$$

From Watson (1944):

$$\int_0^\infty \exp(-p^2x^2) \times J_0(ax)dx = \frac{1}{2p^2}\exp\left(-\frac{a^2}{4p^2}\right) .$$

Thus,

$$f_1(\varepsilon,\sigma) = \frac{\exp-\left(\dfrac{\varepsilon^2 B}{1 + (B\sigma)^2}\right)}{((B\sigma)^2 + 1)^{1/2}} \exp\left(i\left(\frac{B^2\varepsilon^2\sigma}{(B\sigma)^2 + 1} - \tan^{-1}(B\sigma) + \frac{\pi}{2}\right)\right),$$

and Equation (2-17) then gives the sound pressure for a Gaussian source as

$$\bar{p}_1(\varepsilon,\sigma) = \frac{\exp\left(-\dfrac{\varepsilon^2 B}{1+(B\sigma)^2} + \dfrac{\pi}{2}\right)}{((B\sigma)^2+1)^{1/2}} \exp\Bigg(-\alpha r_0 \sigma$$

$$+ i\left(\frac{B^2\sigma\varepsilon^2}{(B\sigma)^2+1} - \tan^{-1}(B\sigma) - \tau\right)\Bigg) . \qquad (2\text{-}19)$$

b. Characteristics of the sound field. With the evaluation of the pressure field radiated by an initial Gaussian amplitude distribution, we will now examine Equation (2-19) more closely to observe some of the characteristics of the field.

(i) Axial response. The effective amplitude of the pressure along the σ axis from Equation (2-19) is

$$\bar{p}_1(0,\sigma) = \frac{\exp(-\alpha r_0 \sigma)}{\sqrt{2}\,((B\sigma)^2+1)^{1/2}} . \qquad (2\text{-}20)$$

In Figure II-1, we plot the value of $\bar{p}_1$ obtained from Equation (2-20) for a Gaussian source (B = 0.4861) with a 0.20 cm radius electrode operating in steel (c_0 = 5840 m/sec) at 6 MHz and with a linear absorption coefficient α equal to 6.9 Nepers. One observes from this figure that the axial amplitude of the Gaussian sound field gradually reduces with distance but it does not exhibit any of the nearfield pressure fluctuations that are usually evident in the case of a piston transducer.

(ii) Beam width. From Equation (2-19) one observes that at different distances σ from the transducer, the sound field across the beam remains proportional to the Gaussian function. Further, it is easy to see that an increase in beam width occurs and is accompanied

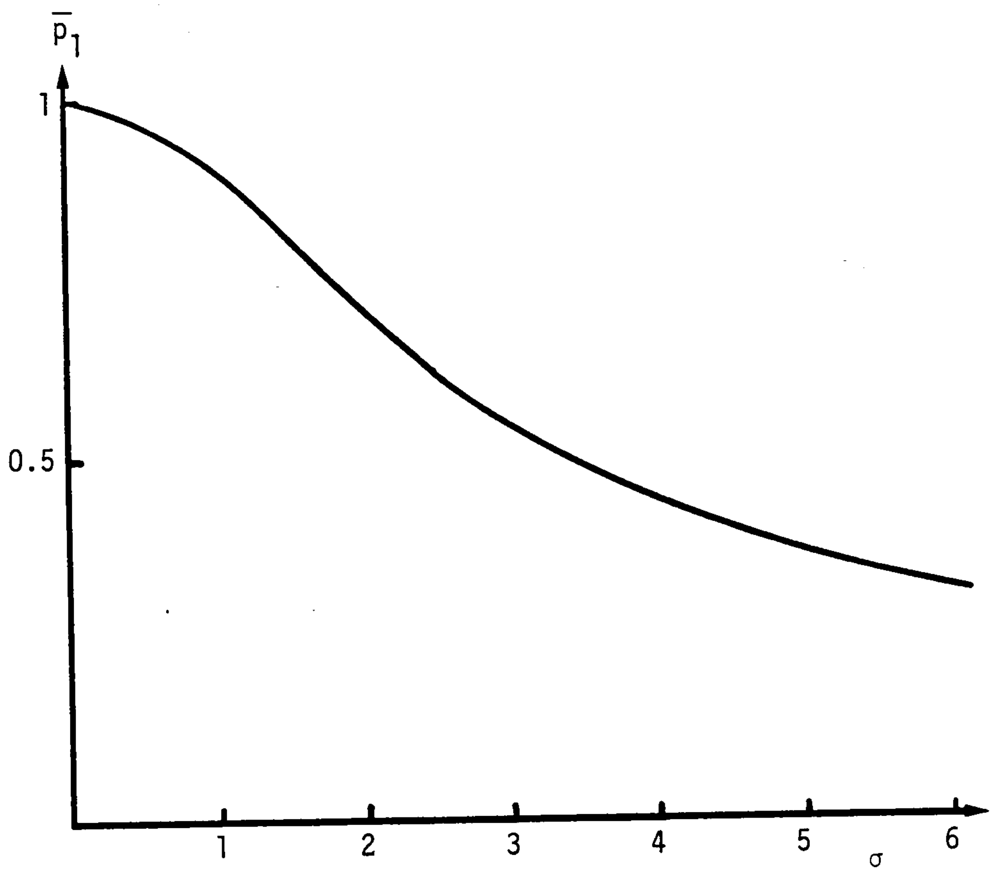

Figure II-1. Normalized sound pressure distribution along the propagation axis.

by a decrease in the amplitude of the wave with propagation distance. This process is pictured in Figure II-2.

c. Average pressure on the receiver. In a through transmission system one can obtain the average pressure on the receiver by integrating Equation (2-19) over the receiver area. This gives:

$$\overline{p}(\tau)_1 = \frac{2}{\pi}\int_{\varepsilon=-a}^{a}\int_{\phi=0}^{2\pi} \frac{\exp\left(\dfrac{-\varepsilon^2 B}{1+(B\sigma)^2}+\dfrac{\pi}{2}\right)}{\left(1+(B\sigma)^2\right)^{1/2}} \exp\left(-i(\tau+\gamma)\right)\varepsilon d\varepsilon d\phi \ , \tag{2-21}$$

where $\gamma = \left(\dfrac{B^2\sigma\varepsilon^2}{1+(B\sigma)^2} - \tan^{-1}(B\sigma)\right)$ is the phase shift.

Integrating Equation (2-21) with respect to ϕ one gets:

$$\overline{p}(\tau)_1 = 8\int_{\varepsilon=0}^{a} \frac{\exp\left(\dfrac{-\varepsilon^2 B}{1+(B\sigma)^2}+\dfrac{\pi}{2}\right)}{\left(1+(B\sigma)^2\right)^{1/2}} \exp\left(-i(\tau+\gamma)\right)\varepsilon d\varepsilon \ . \tag{2-22}$$

Since in the study of attenuation one wishes to measure the maximum pressure, it is necessary to determine the magnitude of Equation (2-22).

Substituting the identity

$$e^{i\theta} = \cos\theta + i\sin\theta \ ,$$

into Equation (2-22) one gets:

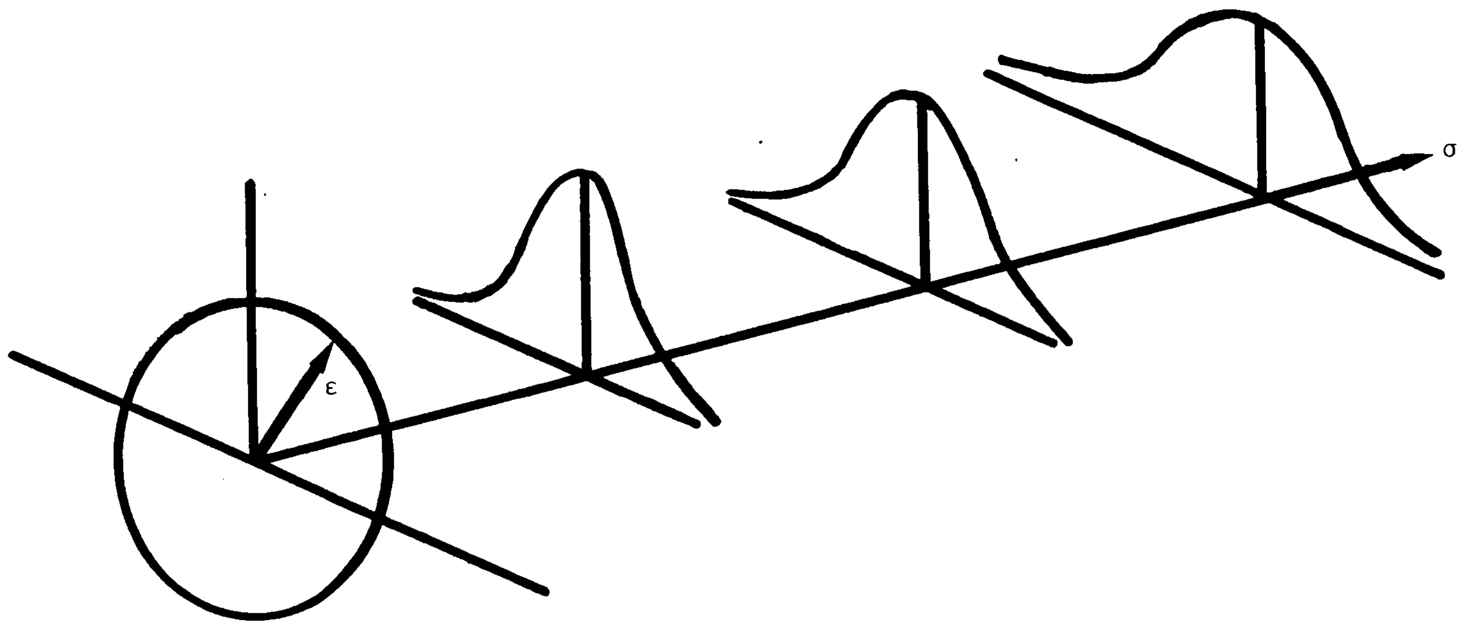

Figure II-2. The shape of the normalized values of pressure in a plane normal to the direction of propagation.

$$\overline{p}(\tau)_1 = 8 \int_0^a \frac{\exp\left(\frac{-\varepsilon^2 B}{1 + (B\sigma)^2} + \frac{\pi}{2}\right)}{(1 + (B\sigma)^2)^{1/2}} \{\cos(\tau + \gamma) - i\sin(\tau + \gamma)\}\varepsilon d\varepsilon \; . \tag{2-23}$$

The real part of Equation (2-23) is:

$$\overline{p}(\tau)_{1r} = 8 \int_0^a \frac{\exp\left(\frac{-\varepsilon^2 B}{1 + (B\sigma)^2} + \frac{\pi}{2}\right)}{(1 + (B\sigma)^2)^{1/2}} \cos(\tau + \gamma)\varepsilon d\varepsilon \; . \tag{2-24}$$

Since cos(A + B) = cosAcosB - sinAsinB, then

$$\overline{p}(\tau)_{1r} = 8 \left\{\int_0^a \frac{\exp\left(\frac{-\varepsilon^2 B}{1 + (B\sigma)^2} + \frac{\pi}{2}\right)}{(1 + (B\sigma)^2)^{1/2}} \cos\tau \cos\gamma \varepsilon d\varepsilon \right.$$

$$\left. - \int_0^a \frac{\exp\left(\frac{-\varepsilon^2 B}{1 + (B\sigma)^2} + \frac{\pi}{2}\right)}{(1 + (B\sigma)^2)^{1/2}} \sin\tau \sin\gamma \varepsilon d\varepsilon \right\},$$

or

$$\overline{p}(\tau)_{1r} = \frac{8}{(1 + (B\sigma)^2)^{1/2}} \left\{ \cos\tau \left[\int_0^a \exp\left(\frac{-\varepsilon^2 B}{1 + (B\sigma)^2} + \frac{\pi}{2}\right) \cos\gamma \varepsilon d\varepsilon\right] \right.$$

$$\left. - \sin\tau \left[\int_0^a \exp\left(\frac{-\varepsilon^2 B}{1 + (B\sigma)^2} + \frac{\pi}{2}\right) \sin\gamma \varepsilon d\varepsilon\right] \right\} \; . \tag{2-24a}$$

Similarly, the imaginary part of $\overline{p}(\tau)_1$ is

$$\overline{p}(\tau)_{1i} = \frac{8}{(1 + (B\sigma)^2)^{1/2}} \left(\cos\tau \left[\int_0^a \exp\left(\frac{-\varepsilon^2 B}{1 + (B\sigma)^2} + \frac{\pi}{2} \right) \sin\gamma\varepsilon d\varepsilon \right] \right.$$

$$\left. - \sin\tau \left[\int_0^a \exp\left(\frac{-\varepsilon^2 B}{1 + (B\sigma)^2} + \frac{\pi}{2} \right) \cos\gamma\varepsilon d\varepsilon \right] \right) . \qquad (2\text{-}24b)$$

Then, the magnitude of $\overline{p}(\tau)_1$ is given by

$$|\overline{p}|_{1n} = [(\overline{p}(\tau)_{1r} + i\overline{p}(\tau)_{1i})(\overline{p}(\tau)_{1r} - i\overline{p}(\tau)_{1i})]^{1/2} ,$$

or

$$|\overline{p}|_{1n} = \frac{8}{(1 + (B\sigma)^2)^{1/2}} (f_1{}^2 + f_2{}^2)^{1/2} , \qquad (2\text{-}25)$$

where

$$f_1 = \int_0^a \exp\left(\frac{-\varepsilon^2 B}{1 + (B\sigma)^2} + \frac{\pi}{2} \right) \cos\gamma\varepsilon d\varepsilon$$

and

$$f_2 = \int_0^a \exp\left(\frac{-\varepsilon^2 B}{1 + (B\sigma)^2} + \frac{\pi}{2} \right) \sin\gamma\varepsilon d\varepsilon .$$

By integrating f_1 and f_2 one is able to obtain the analytical expressions:

$$f_1 = \frac{\exp\left(\frac{-Ba^2}{1 + (B\sigma)^2} \right)}{2} \left(\frac{\cos B^2\sigma a^2}{1 + (B\sigma)^2} \left[\frac{-\cos(\tan^{-1}(B\sigma))}{B} \right. \right.$$

$$\left. \left. - \sigma\sin\left(\tan^{-1}(B\sigma)\right) \right] + \frac{\sin B^2\sigma a^2}{1 + (B\sigma)^2} \left(\sigma\cos(\tan^{-1}(B\sigma)\right) \right.$$

$$+ \frac{\sin(\tan^{-1}(B\sigma))}{B}\Bigg) + \frac{1}{2}\left(\frac{\cos(\tan^{-1}(B\sigma))}{B}\right.$$

$$\left. + \sigma\sin\left(\tan^{-1}(B\sigma)\right)\right) , \qquad (2\text{-}25a)$$

$$f_2 = \frac{\exp\left(\frac{-Ba^2}{1 + (B\sigma)^2}\right)}{2}\left(\frac{\cos B^2\sigma a^2}{1 + (B\sigma)^2}\left(-\sigma\cos\left(\tan^{-1}(B\sigma)\right)\right.\right.$$

$$\left. + \frac{1}{B}\sin\left(\tan^{-1}(B\sigma)\right)\right) + \frac{\sin B^2\sigma a^2}{1 + (B\sigma)^2}$$

$$\left.\left(-\frac{1}{B}\cos\left(\tan^{-1}(B\sigma)\right) - \sigma\sin\left(\tan^{-1}(B\sigma)\right)\right)\right)$$

$$+ \frac{1}{2}\left(\sigma\cos\left(\tan^{-1}(B\sigma)\right) - \frac{1}{B}\sin\left(\tan^{-1}(B\sigma)\right)\right) . \qquad (2\text{-}25b)$$

This equation then represents a mathematical diffraction model which gives the maximum pressure impinging on a circular transducer when a pressure wave of magnitude 1 is reflected n times from the lower surface of a sample with parallel faces.

d. Diffraction correction factor. From the preceding analysis, an amplitude correction factor $(DC)_n$ can now be defined as the ratio of the magnitude of the maximum pressure at a receiver of radius a when an infinite plane wave is impinging on its surface ($|\bar{p}|_1 = 1$) to the situation described by Equation (2-25). This gives:

$$(DC)_n = \frac{1}{|\bar{p}|_{1n}} . \qquad (2\text{-}26)$$

After n reflections from the lower face of a specimen the magnitude of the maximum pressure $|\bar{p}|_{1n}$ can be used in Equation (2-26) to obtain the diffraction correction. The diffraction correction then is multiplied by the measured pressure amplitude of the nth pulse to obtain the corrected pressure amplitude:

$$|p_C|_n = |p|_n \times (DC)_n \;. \qquad (2\text{-}27)$$

B. Geometrical Correction Model

As has been pointed out, measurements of ultrasonic attenuation can be affected seriously by the lack of parallelism between the transducer and reflector. Thus, it has been found that one can observe a significant deviation of the pulse height resulting from diffraction in the presence of a wedge angle. A mathematical model now will be presented to explain the simultaneous effects of diffraction and non-parallelism on the echo train. For convenience this is referred to as the geometrical model.

1. General Description of Wave Propagation in a Wedged Sample

As shown in Figure II-3, let us assume that a source of ultrasonic waves having radial symmetry about origin O is located on the top surface of a sample at t = 0. The center of the wave will travel along the path of a ray through the sample, reflect from the opposite sample-air interface for t > 0. This process will continue until all the energy contained by the wave is dissipated within the sample. With each successive reflection from the lower face, the relative angle γ_n between

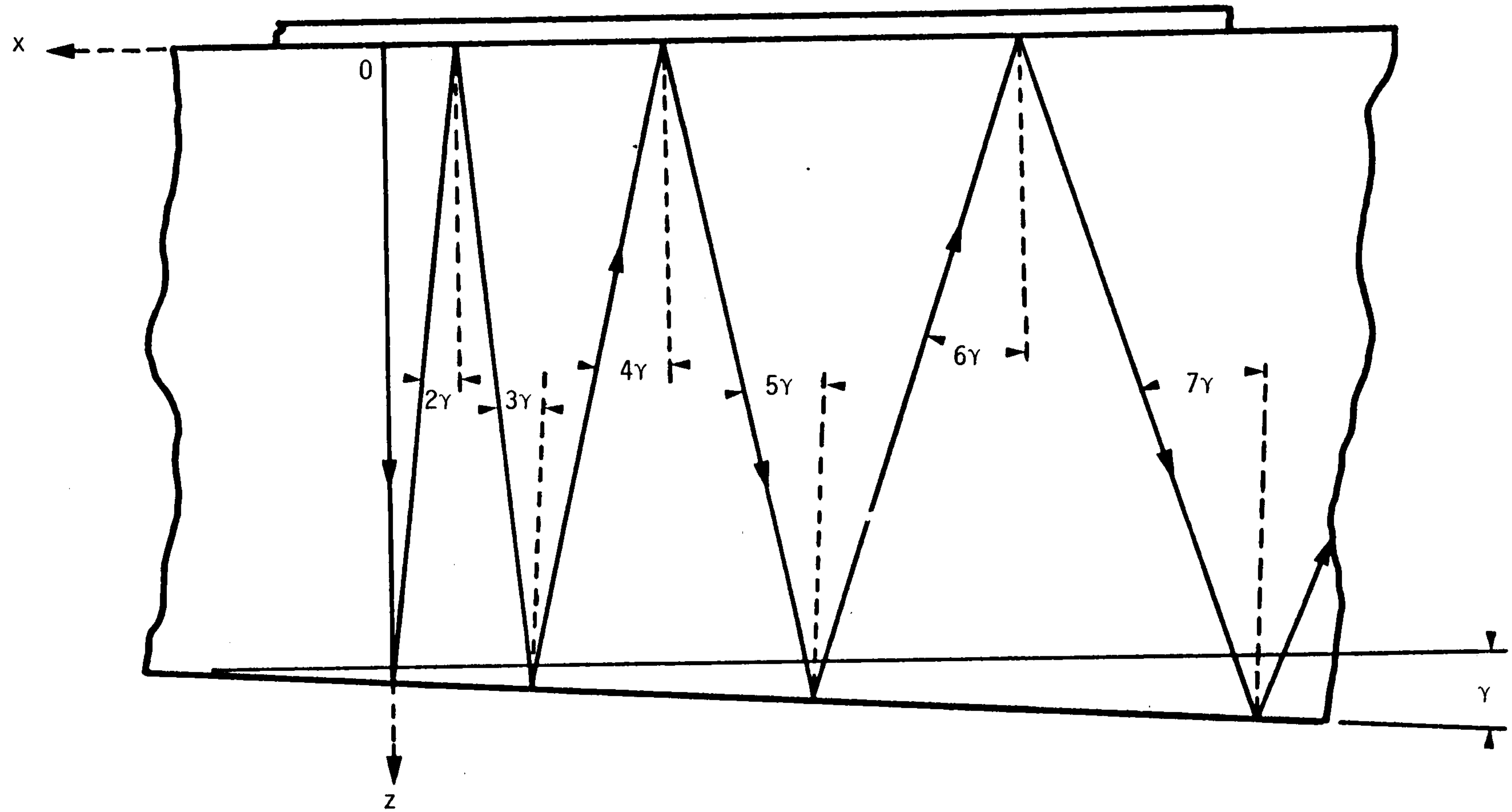

Figure II-3. Propagation path of the center of the disturbance.

the upper surface and the axis of the ultrasonic beam is increased by 2γ. After n reflections, the relative angle is given by

$$\gamma_n = 2n\gamma \ . \tag{2-28}$$

As Equation (2-28) represents the angle between the wave front and the transducer, the variation of phase that the transducer sees across its surface as a function of the nondimensional coordinate ε from its center is $\varepsilon \sin\gamma_n$.

2. Average Pressure on the Receiver

From the expressions for the pressure at a point in the field expressed by Equation (2-19) and the variation of phase across the transducer one can now obtain an equation which describes the change of pressure across the transducer after n reflections. This gives:

$$\bar{p}(\tau)_1 = \frac{\exp\left(\dfrac{-\varepsilon^2 B}{1 + (B\sigma_1)^2} + \dfrac{\pi}{2}\right)}{((B\sigma_1)^2 + 1)^{1/2}} \exp\left(-i\left(\tau - \frac{B^2\sigma_2\varepsilon^2}{1 + (B\sigma_2)^2} - \tan^{-1}(B\sigma_2)\right)\right) \tag{2-29}$$

Here $\sigma_1 = 2n\sigma$ and $\sigma_2 = \sigma_1 - \varepsilon\sin\gamma_n$. Integrating Equation (2-29) over the area of a receiver one finds that the magnitude of average pressure on the receiver is:

$$|\bar{p}|_{1n} = \frac{8}{(1 + (B\sigma_1)^2)^{1/2}} (f_1^{\,2} + f_2^{\,2})^{1/2} \ , \tag{2-30}$$

where

$$f_1 = \int_0^a \exp\left[\frac{-\varepsilon^2 B}{1 + (B\sigma_1)^2} + \frac{\pi}{2}\right] \cos\left[\frac{B^2\sigma_2\varepsilon^2}{1 + (B\sigma_2)^2} - \tan^{-1}(B\sigma_2)\right] \varepsilon d\varepsilon \tag{2-30a}$$

and

$$f_2 = \int_0^a \exp\left[\frac{-\varepsilon^2 B}{1 + (B\sigma_1)^2} + \frac{\pi}{2}\right] \sin\left[\frac{B^2\sigma_2\varepsilon^2}{1 + (B\sigma_2)^2} - \tan^{-1}(B\sigma_2)\right] \varepsilon d\varepsilon \ . \tag{2-30b}$$

It should be noted that Equation (2-30) must be numerically integrated in order to find its value as no analytical form of this integration has been found.

Accordingly, $|\bar{p}|_{1n}$ in this model represents the maximum pressure impinging on a transducer when a pressure wave is subjected to geometrical attenuation and is of magnitude of 1 when reflected n times from the lower face of a wedged sample. Furthermore, the expression for $|\bar{p}|_{1n}$ combines both the results of diffraction theory and phase cancellation from nonparallelism in describing the effects of these factors on the observed echo pattern.

3. Geometrical Correction Factor

One is now in a position to define a geometrical correction factor (DCG)n which represents the ratio of the magnitude of the average pressure felt on a receiver of radius a when an infinite plane wave is striking its surface ($|\bar{p}|_1 = 1$) to that given by Equation (2-30). This correction factor is given by

$$(DCG)_n = \frac{1}{|\bar{p}|_{1n}} \ . \tag{2-31}$$

After n reflections from the lower surface of a wedged sample the magnitude of the maximum pressure $|\bar{p}|_{1n}$ can be corrected for the effects of both nonparallelism and diffraction to obtain a corrected maximum pressure $|p_{CG}|_n$:

$$|p_{CG}|_n = |p|_n \times (DCG)_n \ . \qquad (2\text{-}32)$$

A computer program written in the Basic language which corrects amplitude measurements for both nonparallelism and diffraction using the correction factor detailed in Equation (2-31) is given in Appendix B. The input variables for this program are: DAT(NN,2) the uncorrected pressure amplitude measurements, BG the Gaussian coefficient, CO the velocity of sound in the sample, F4 the frequency of the ultrasonic waves, WA the wedge angle, TS the sample thickness, A6 the radius of the Gaussian electrode and A8 the radius of the receiving transducer.

CHAPTER III

APPARATUS, SAMPLES, AND PROCEDURES

A. Experimental Considerations

The purpose of this investigation is to extend our understanding of diffraction and nonparallelism in precise attenuation measurements. In order to accomplish this aim we used the through-transmission technique of ultrasonic testing. The rationale behind this particular selection of technique was twofold: First, it allows us to make use of the attractive characteristics of the Gaussian transducer in a transmitting mode, viz., a relatively narrow beam free of sidelobes and free of the maxima and minima that characterize the beam generated by a piston transducer. Secondly, the technique provides us with the possibility to use a large transducer to receive the integrated pressure in the field of the Gaussian transducer so that we could handle the nonparallelism and diffraction problem in a simple fashion.

The resonant frequencies of the Gaussian transducers were 1, 2, and 3 MHz. It was found that by using odd overtones of these resonant frequencies we could get measurements in the usual NDT testing frequency range and simultaneously satisfy the D/T conditions necessary for producing a Gaussian amplitude distribution on the transmitter (Du and Breazeale, 1984).

B. Electrical System

A block diagram of the circuit used in this study is given in Figure III.1. In this circuit the H/P pulse function generator is operated in the internal burst mode. The output is a tone burst which may be controlled as to its length, voltage level, and frequency.

The signal generated by the function generator is applied to the transmitting transducer. As a consequence of the piezoelectric effect, this transducer produces a stress wave in the sample. This wave passes through the sample and is detected by a receiving transducer. The receiving transducer reconverts the mechanical vibrations into an electrical signal which is transmitted to the receiver. The receiver contains a wide band (1 to 90 MHz) amplifier which is capable of amplifying the RF signals up to 20 decibels. The signal is then detected and amplified by the second stage of the receiver up to 70 decibels. Subsequently, it is fed into a boxcar integrator and displayed on the oscilloscope. The synchronization of the entire system is ensured by triggering all the instruments by the function generator. A 50 ohm terminator is used to provide impedance matching between the function generator and the transmitting transducer. An impedance matching unit matches impedances in the receiver transducer circuit.

C. Transducers

1. Transducer Construction

Quartz 2.54 cm in diameter X-cut crystals are used both as the transmitters and receivers of the ultrasonic waves. These crystals

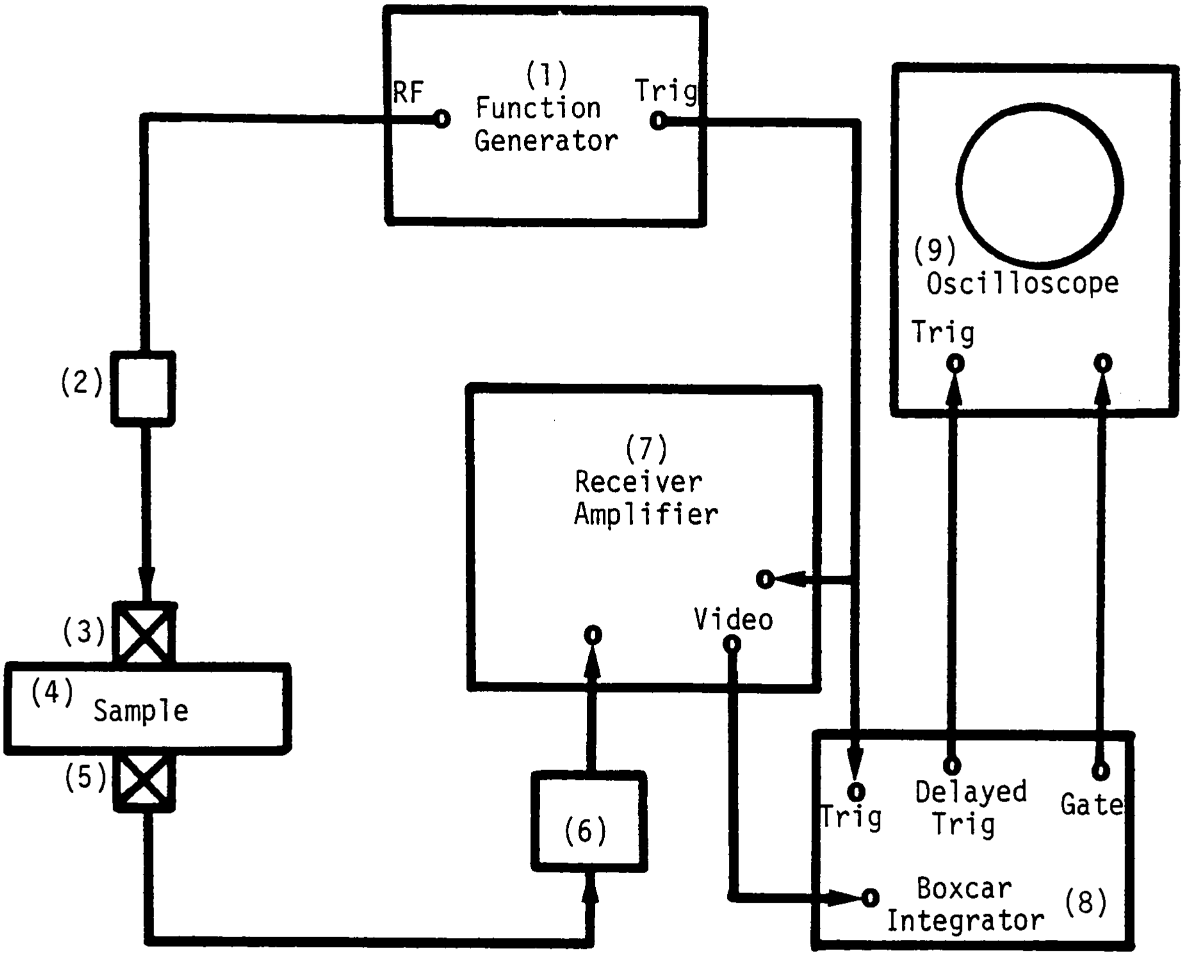

(1) HP Pulse/Function Generator Model 8116A
(2) Tektronix 50Ω Terminator
(3) Gaussian Transducer
(4) Steel Plate
(5) Receiving Transducer
(6) Matec Impedance Matching Network Model 60
(7) Matec Model 6600, Plug In Type 750
(8) Princeton Appl. Res. Model 160
(9) HP Model 1740A (100 MHz)

Figure III-1. Electrical circuit used in attenuation study.

were placed in lucite housings which were in the form of a ring with a depression where the crystals could be inserted. The lucite rings were positioned in brass transducer housings and pressure was applied by means of a vise to the housings. This is pictured in Figure III.2. A detailed breakdown of the various components that comprise the transducer is shown in Figure III.3. The brass housings in the figure had been previously used in immersion testing (see Scott, 1975). To ensure parallelism between the crystals and sample faces and to damp the crystals to avoid the "ringing" effect described by Krautkramer (1977), the crystals were wrung onto the sample using stopcock grease and stopcock grease was applied on the rear surfaces of the crystal.

2. Electrical Operation

The electrical signal from the H/P function generator enters the BNC connector of the transmitting transducer housing. This signal is fed to a circular brass cylinder which is positioned in a lucite cylinder. The brass cylinder serves as the electrode in this transducer and has been manufactured to the dimensions required by the theory in Appendix A to produce a Gaussian amplitude distribution at the surface of the crystal as a result of electrical fringing. The stress wave passing through the sample is received by a receiving transducer located on the opposite face of the sample. The mechanical vibrations of the receiving crystal produce an electrical signal which is picked up by a spring loaded retractable connector which is in contact with

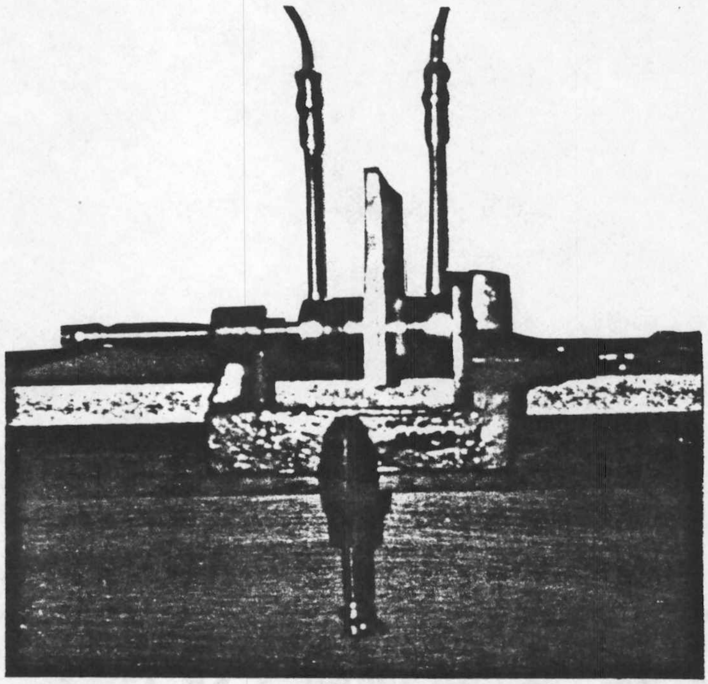

Figure III-2. Ultrasonic measurement setup showing the steel plate, transducers, and the vise.

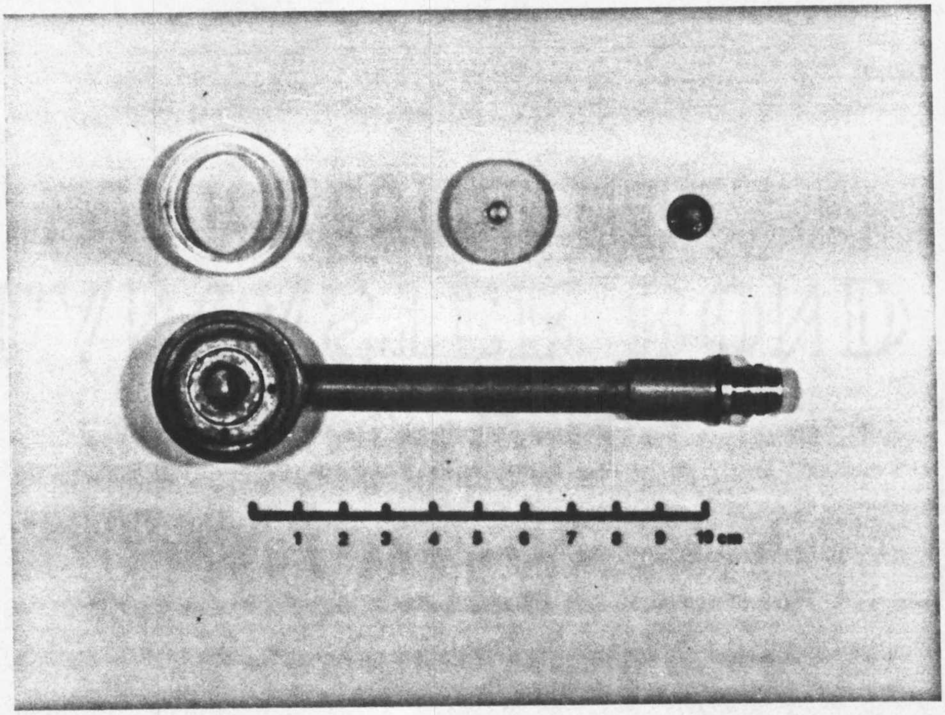

Figure III-3. Transducer parts. Top row, left to right: lucite housing ring, teflon cylinder housing and electrode. Bottom row: main brass housing.

the electrode[1] attached to the surface of the crystal. The electrical signal then is fed through the BNC connector of the receiving transducer housing to the receiver. To complete the circuit a brass connector is used to provide a ground connection to the lower face of the crystal.

D. Samples

In our preliminary investigation attenuation measurements were conducted on a steel plate which had been manufactured for a previous study (Boudreault, 1982). During the course of this work we found that the number of echoes received was not sufficient to evaluate our geometrical model in an adequate fashion. To facilitate a more detailed evaluation, thinner samples were made: one by the Canadian Forces Aerospace Maintenance Development Unit (CFAMDU) and one by Oak Ridge National Laboratory (ORNL). Surfaces of both samples were precision flats ground at increments of 6 minutes of arc up to one degree. Detailed ultrasonic investigations of the samples, however, revealed the presence of secondary echoes from inhomogeneities within the CFAMDU sample. Consequently it was decided to concentrate our efforts on the ORNL sample which gave a clean echo pattern in order to evaluate the technique used in this thesis for determining the magnitude of geometrical losses from nonparallelism and diffraction. The CFAMDU sample is being retained for further tests to be made after

[1]A silver electrode was plated on the crystal surface.

the technique has been evaluated under the more ideal situation possible with the ORNL sample.

The ORNL sample is a plate of AISI Type A-2 Tool Steel. This material was selected because of its isotropy, low attenuation coefficient at the frequency range used, and good machinability.

The sample plate was first machined to ensure parallelism of the upper and lower faces and to eliminate surface defects. The upper face was then ground in 11 facets of approximately 1 inch in width with an increasing relative angle between facets. A drawing of the sample which illustrates the geometry and the coordinate system used in the mathematical characterization is shown in Figure III-4. One notes in this figure that the Z direction corresponds to wave propagation direction, Y direction to the width of the sample, and X direction to the lateral displacement of the propagating wave.

E. Sequence of the Investigation

The first step in this investigation involved the characterization of the sample. This activity required that we make accurate measurements of:

1. the various angles of the facets on the sample;
2. thickness of the sample; and
3. the velocity of ultrasonic waves within the sample.

With the completion of these details one then could proceed with measurement of attenuation. The detailed procedures are presented in the following paragraphs.

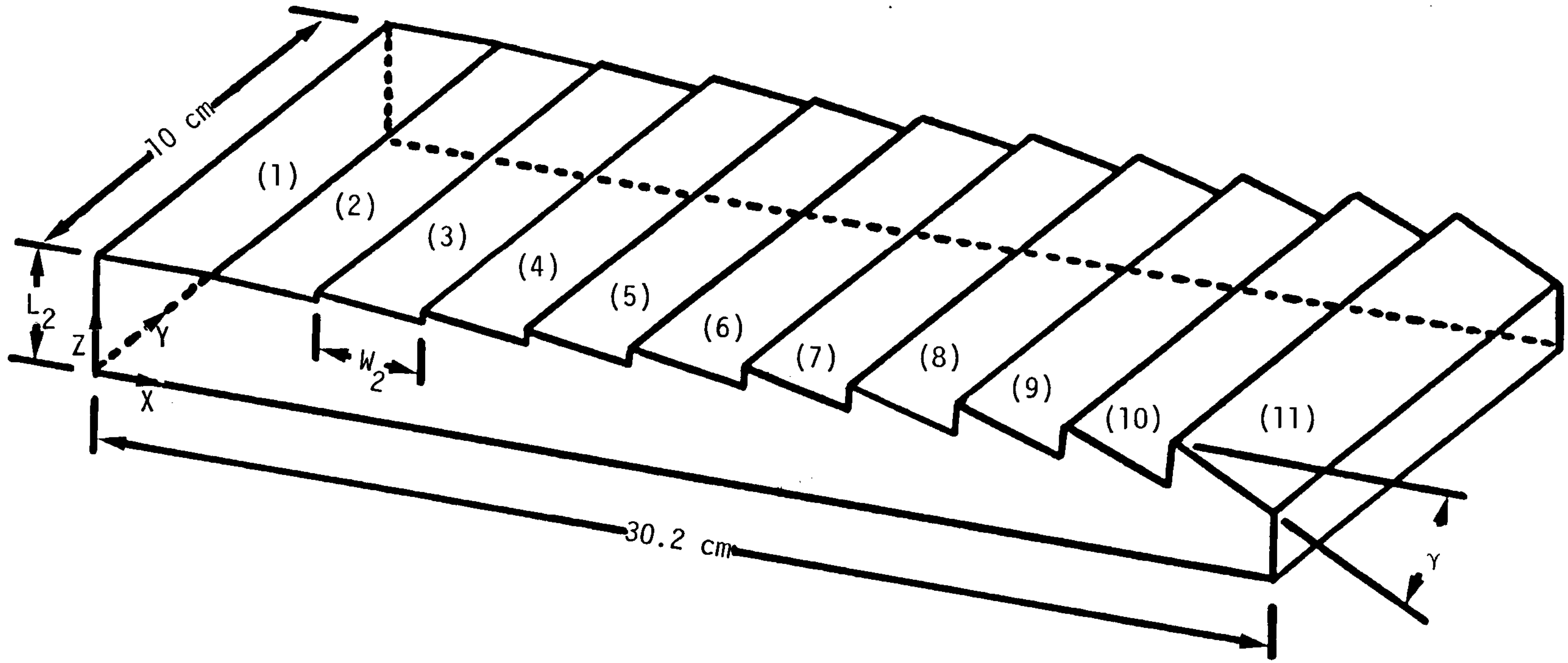

Figure III-4. Geometry of the wedged sample.

1. Sample Characterization

The angles of the facets of the sample were measured by a collimator and two optically flat reflectors as shown in Figure III.5. As a first step a reflector is wrung onto the lower surface of the sample. Light originating in the Gauss eyepiece of the collimator is then reflected from this reflector thereby forming an image of the cross hairs in the focal plane of the collimator. The cross hairs on the micrometer are aligned with this image and the micrometer reading is noted. Subsequently, a parallel reflector is wrung onto the edge of the upper surface of the sample and the micrometer cross hairs are moved until they line up with the image from the upper surface.

The wedge angle of the facet is then determined by using the following relationship:

$$\gamma = \frac{\sin^{-1}(\Delta x/f)}{2}$$

where

γ = wedge angle;

f = focal length[1] of the collimator - 29.84 cm; and

Δx = distance between the two image positions.

Angle measurements employing this procedure are successively carried out on each of the facets at both edges of the sample ($y = 0$ cm and $y = 10$ cm locations).

The sample thickness is measured by using a Starrett dial indicator. Readings of the thickness were taken at the y position

---

[1]The value of f, the focal length, was found by using the Newtonian method as detailed by Palmer (1969).

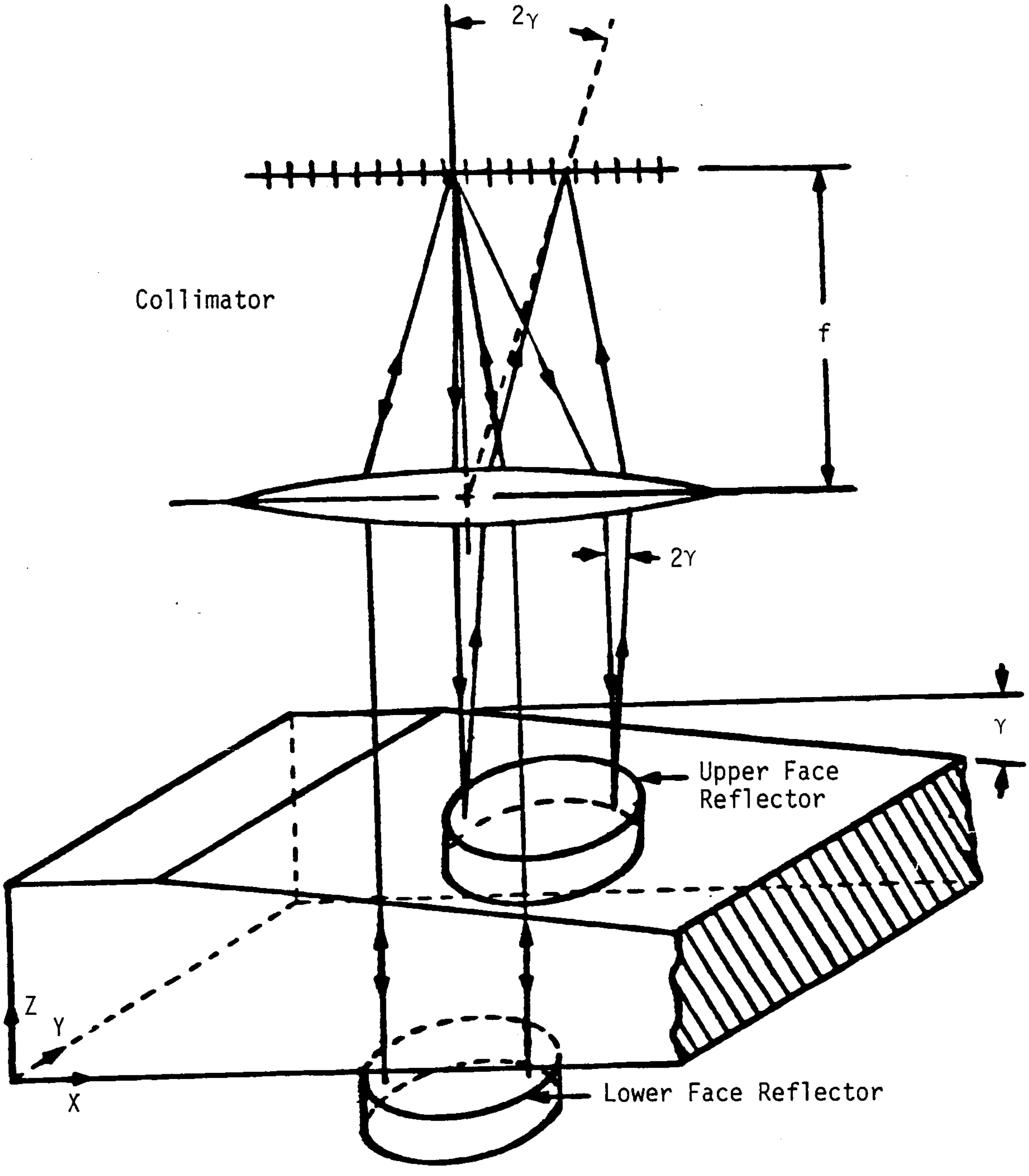

Figure III-5. Schematic of optical measurement setup.

corresponding approximately to the center of the transducer ($y = 2$ cm and $y = 8$ cm). The resultant angle and thickness are shown in Table III.1.

2. Velocity Measurements

Measurement of the velocity of the ultrasonic waves is made by using the pulse interference technique. The experimental setup for this technique is illustrated in Figure III.6. In this arrangement the Hewlett-Packard function generator is replaced by an Arenburg pulsed amplifier. A frequency counter, CW generator, and decoupler limiter are also added to the circuit. The pulsed amplifier is used in this setup because of its capability to be operated in a double pulse mode allowing one to generate two pulses whose spacing in time causes them to interfere at the receiving transducer. The decoupler sends electrical signals to the transducer and oscilloscope and limits the amplitude of the signal fed to the oscilloscope.

As a first step in the velocity measurements, the surface of the sample is cleaned with acetone. Subsequently, a drop of couplant (nonaq stopcock grease) is applied to the sample and the transducers are mounted by applying pressure to the housing by use of a vise. Once a suitable single-pulse echo pattern is evident on the oscilloscope, the fundamental frequency[1] of the crystal is found by changing the frequency on the CW generator until minimum attenuation of the

[1]The fundamental frequency of the crystal used for the velocity measurements was 4 MHz.

Table III.1

Sample Geometry Data[a]

Facet No.	$\gamma_{No.}$ (milliradians)[b]		$L_{No.}$ (cm)[c]	
	y = 0.0 cm	y = 10.0 cm	y = 2 cm	y = 8 cm
1	0.22	0.21	0.9220	0.9243
2	2.34	2.98	0.9218	0.9218
3	3.62	3.62	0.9169	0.9169
4	5.32	4.89	0.9144	0.9144
5	7.23	7.45	0.9149	0.9149
6	9.51	10.00	0.9121	0.9106
7	10.43	10.64	0.0119	0.9116
8	11.49	11.70	0.9081	0.9081
9	14.04	13.83	0.9027	0.9017
10	15.75	15.96	0.9068	0.9068
11	18.07	17.31	0.9017	0.9004

[a]The variations of $\gamma_{No.}$ and $L_{No.}$ in the y direction were caused by machining.

[b]Accuracy of these measurements is $\pm 3 \times 10^{-2}$ milliradians.

[c]Accuracy of these measurements is $\pm 5 \times 10^{-5}$ cm.

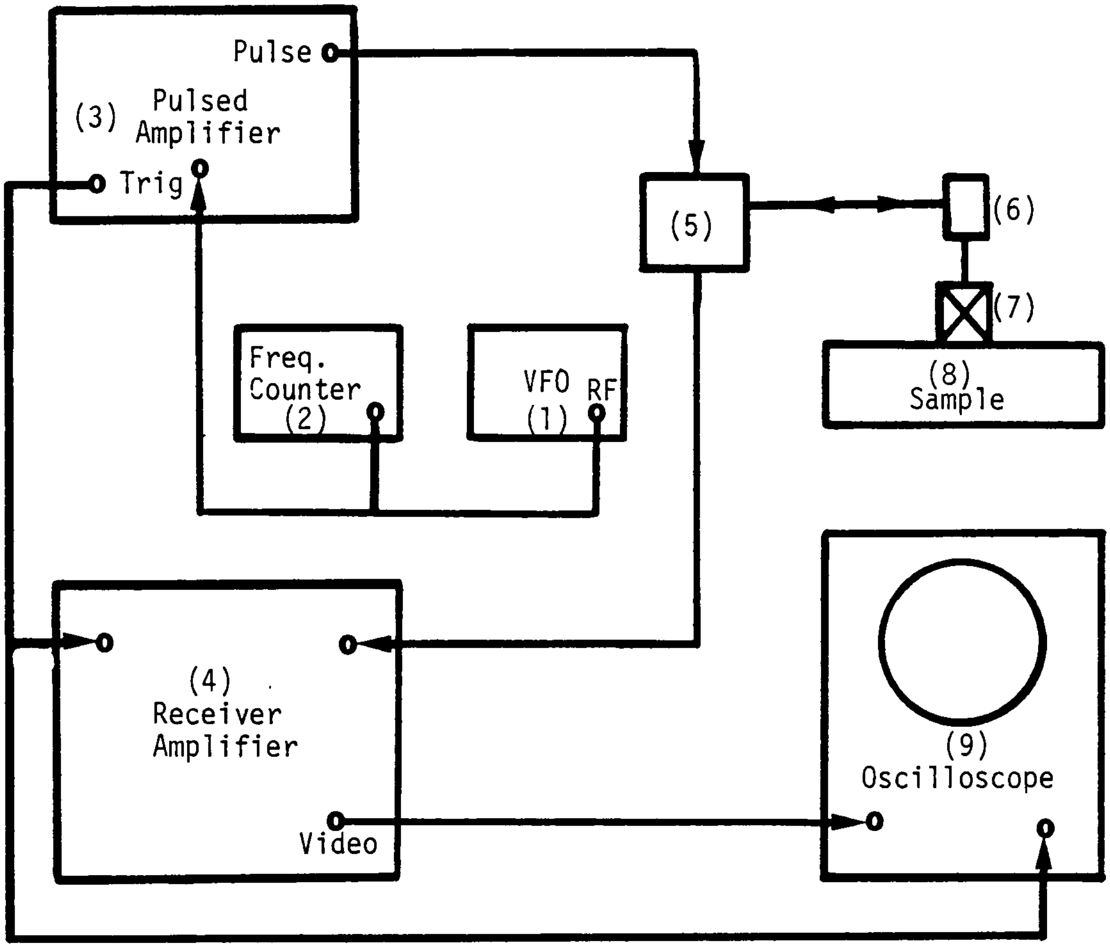

(1) General Radio Model 1211
(2) General Radio Type 1192-B
(3) Arenberg Model PG-650C
(4) Matec Model 6600, Plug In Type 750
(5) Decoupler Limiter
(6) Tektronix 93Ω Terminator
(7) Transducer
(8) Steel Plate
(9) HP Model 1740A (100 MHz)

Figure III-6. Electrical circuit used for velocity measurements.

echo pattern is observed. The gated pulsed amplifier is then put into its double pulse mode. This results in the display of two echo trains on the oscilloscope. By means of the time "delay" potentiometer on the gated amplifier, the time delay between these two pulse trains is adjusted until the trains interfere with one another. The frequency of the VFO is then varied so that the overlapping echoes went through several interference maxima and minima. The number of minima is counted and the initial and final frequencies noted. The velocity is then calculated from

$$V = \frac{2\Delta fL}{\Delta n} ,$$

where Δf is the change in frequency corresponding to a change in peak number Δn, and L is the length of the sample. The average velocity obtained from twelve sets of readings was 0.5549 cm/μsec with a standard deviation of 0.26%. A correction for the losses arising from the transducer and transducer coupling to the sample was calculated and found to be 80 times smaller than the standard deviation. Consequently, this correction was considered negligible and was not applied to the velocity measurements.

3. Attenuation Measurements

The attenuation measurements were made using the circuit shown in Figure III.1 (p. 27). The preparatory procedures used for the attenuation study were the same as those used for velocity measurements up to the establishment of a suitable echo pattern.

Once these were done, the pulse parameters were adjusted to produce echoes with minimum distortion and no signs of interfering with each other. The width of the gate of the boxcar was then adjusted to cover the top of the echo to be measured. Subsequently, the first echo's amplitude was adjusted to a given reference level and the amplitudes of the remaining echoes were measured relative to that of the first echo by use of the boxcar integrator. This procedure was repeated on each facet.

CHAPTER IV

RESULTS AND DISCUSSION

In this chapter we report a series of amplitude measurements that was made using the procedures described in Chapter III. The results were obtained by concentrating our attention on the dependence of the echo train on frequency and wedge angle. The Gaussian transducer described in Appendix A was used in conjunction with a large receiving transducer to measure ultrasonic pulse echo amplitudes in the steel sample from ORNL. The effect of diffraction and changes in wedge angle on the echo train using this configuration is the subject of the following section.

A. Echo Pattern with Gaussian Transducer

In the first segment of this investigation we examine the character of the echo pattern obtained with a Gaussian transmitting transducer. Observation of the diffraction field of this transducer had led us to anticipate an improvement over the echo pattern of the usual piston transducer because the Gaussian field lacks the maxima and minima which are known to characterize the field of a piston transducer. Moreover, it was felt that these attractive features would make the echo pattern variation with wedge angle simpler to calculate. The results of our investigations confirmed these expectations as will be shown.

The echo pattern observed with zero wedge angle displayed an exponential decrease in amplitude as a function of propagation distance and did not exhibit amplitude fluctuations at any of the test frequencies between 2 and 6 MHz. A typical echo train is shown in Figure IV-1. Even with a wedge angle the pattern continued to exhibit a monotonic decrease of amplitude. As the wedge angle increased, a decrease in the number of echoes in the pattern became evident, but the monotonic behavior continued. This is shown in Figure IV-2. For comparison, Figure IV-3 is an echo train for a piston transducer taken under similar conditions (Boudreault, 1982) which does not show a monotonic decrease of amplitude.

B. Pressure Amplitude Corrections

The simplification of the behavior of the echo pattern suggests that it now may be possible to make a quantitative description of the losses resulting from the presence of a wedge angle between the Gaussian transducer and receiving transducer. By correcting the magnitude of each pulse for this effect one should be able to evaluate the intrinsic attenuation in the sample.

In Chapter II we pointed out that one can evaluate the intrinsic attenuation by correcting the pressure amplitude measured experimentally at an echo n in the echo pattern for geometrical losses and using this corrected pressure in the expression given by Equation (2-5) which is repeated for convenience:

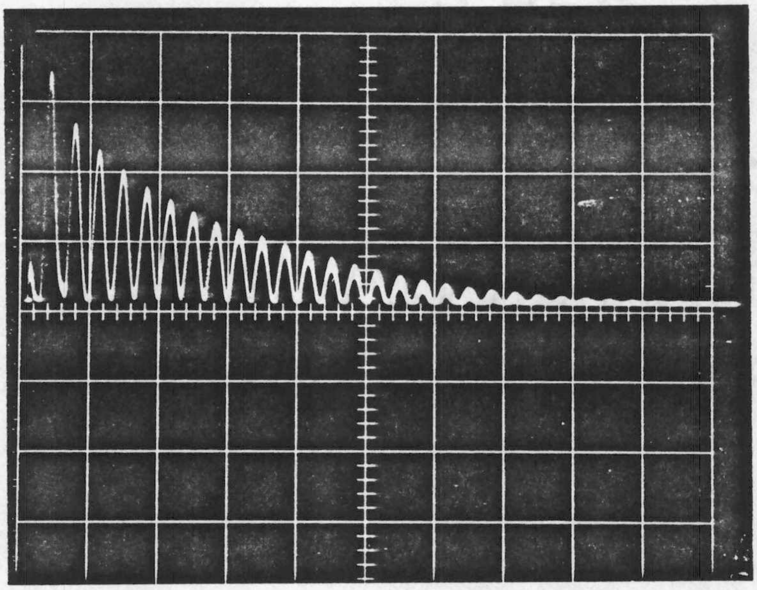

Figure IV-1. Exponential decay pattern at 6 MHz for 0 wedge angle.

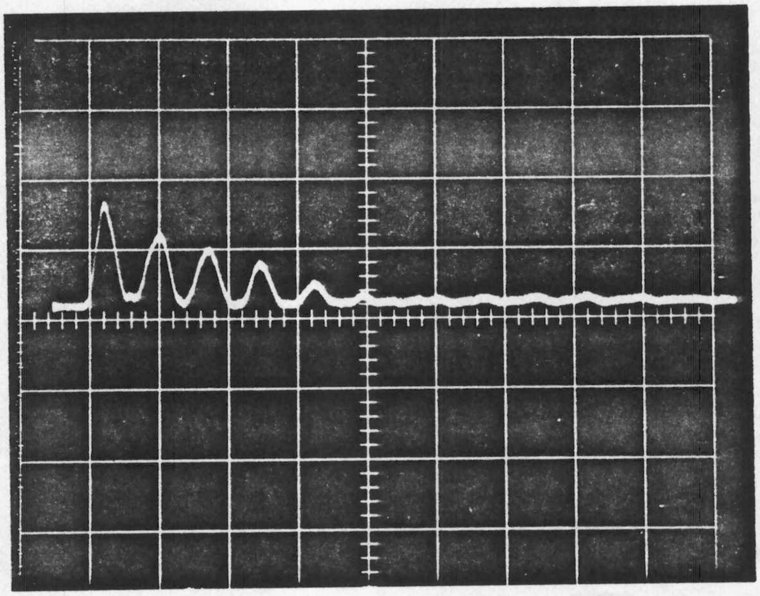

Figure IV-2. Echo train at 3 MHz for $\gamma = 9.51 \times 10^{-3}$ radians.

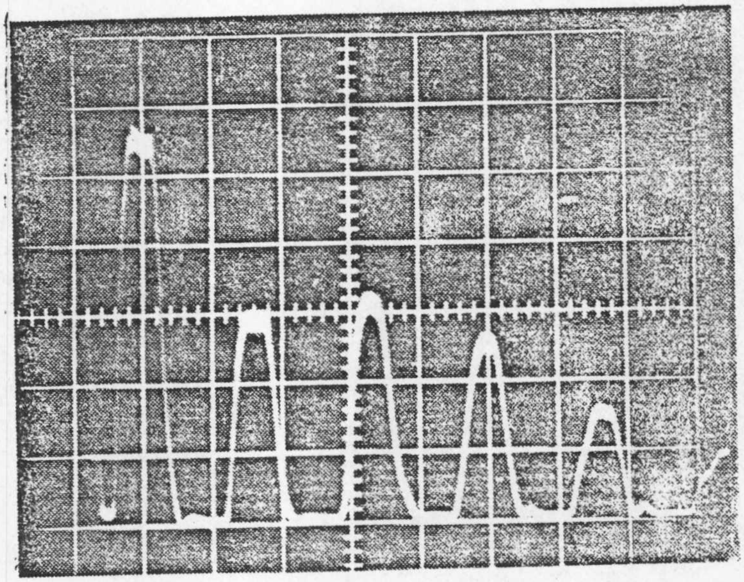

Figure IV-3. Fluctuations in the echo pattern observed at 3 MHz.

Source: J. P. S. Boudreault, "Effect of Nonparallelism on the Measurement of Ultrasonic Attenuation in Solids," Master's thesis, The University of Tennessee, Knoxville, 1982.

$$\alpha = \frac{20}{\Delta x} \log_{10} \left(\frac{p_0}{p_{max}(x)} \right) , \tag{4-1}$$

where p_0 is the measured pressure amplitude of the first echo and the remaining terms in this equation are as previously defined in Chapter I.

If one uses uncorrected data in Equation (4-1) one evaluates the apparent attenuation. Figures IV-4 and IV-5 are examples of the apparent attenuation for two of the frequencies investigated. The apparent attenuation for each echo is different (but the intrinsic attenuation for each echo would be the same, of course). The apparent attenuation of the first echo is not given in these plots because the amplitude of the first echo is used as the reference value p_0. As can be seen, the apparent attenuation of each echo is a strong function of the wedge angle. At zero wedge angle, however, the apparent attenuation of each echo may be corrected for diffraction to give the intrinsic attenuation which is the same for each echo. This is the subject of the next section.

1. Diffraction Correction for Zero Wedge Angle

In Chapter II a model was presented that enables one to correct experimental values of pressure amplitudes of each echo for diffraction within the limit of validity of the parabolic approximation. This model now is applied to adjust the amplitude values obtained from zero angle measurements at a frequency of 6 MHz. At this frequency the Gaussian transducer used had a valve Ka = 15, which satisfies the parabolic approximation requirements quite well. The corrected attenuation values

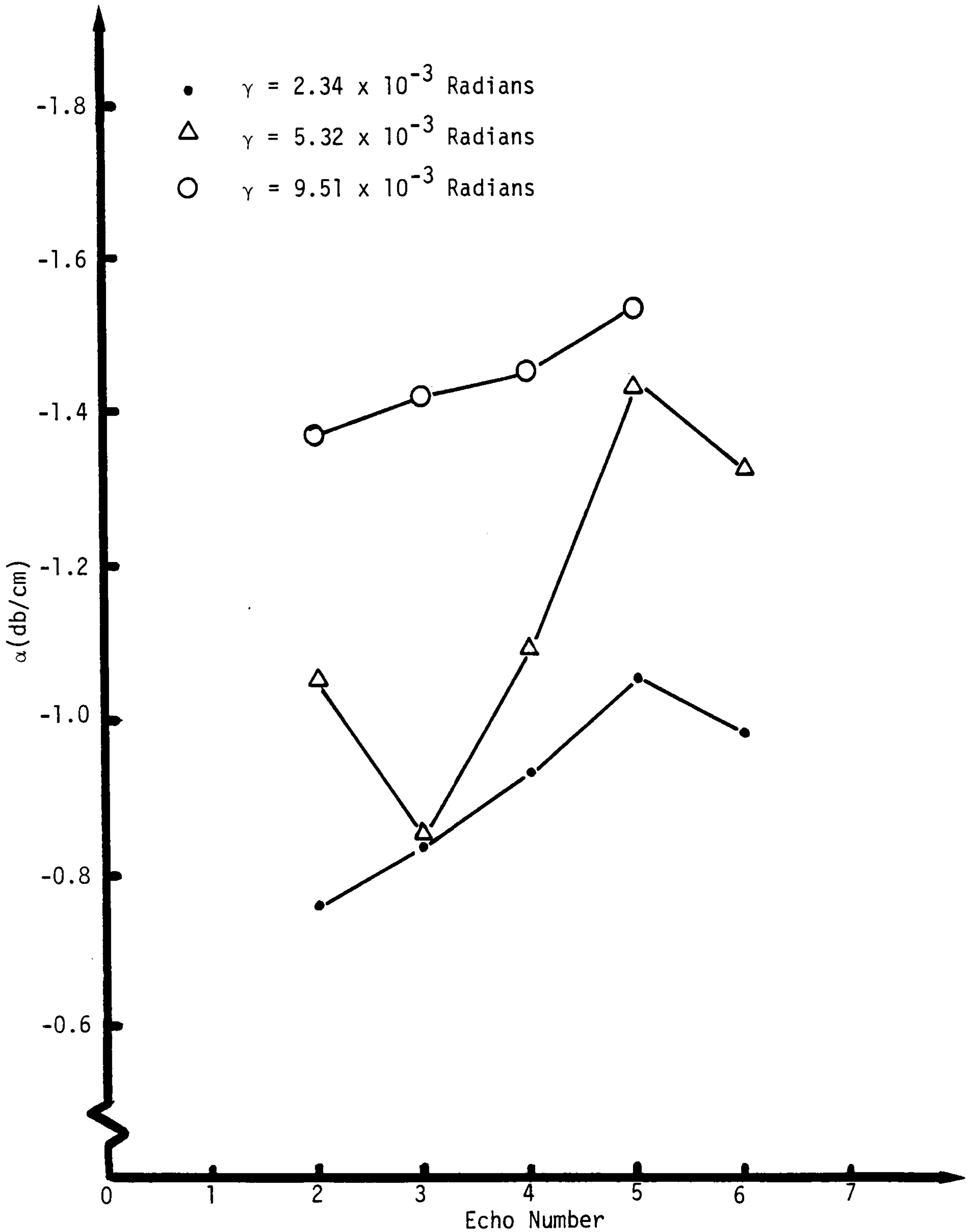

Figure IV-4. Apparent attenuation at 3 MHz for different wedge angles.

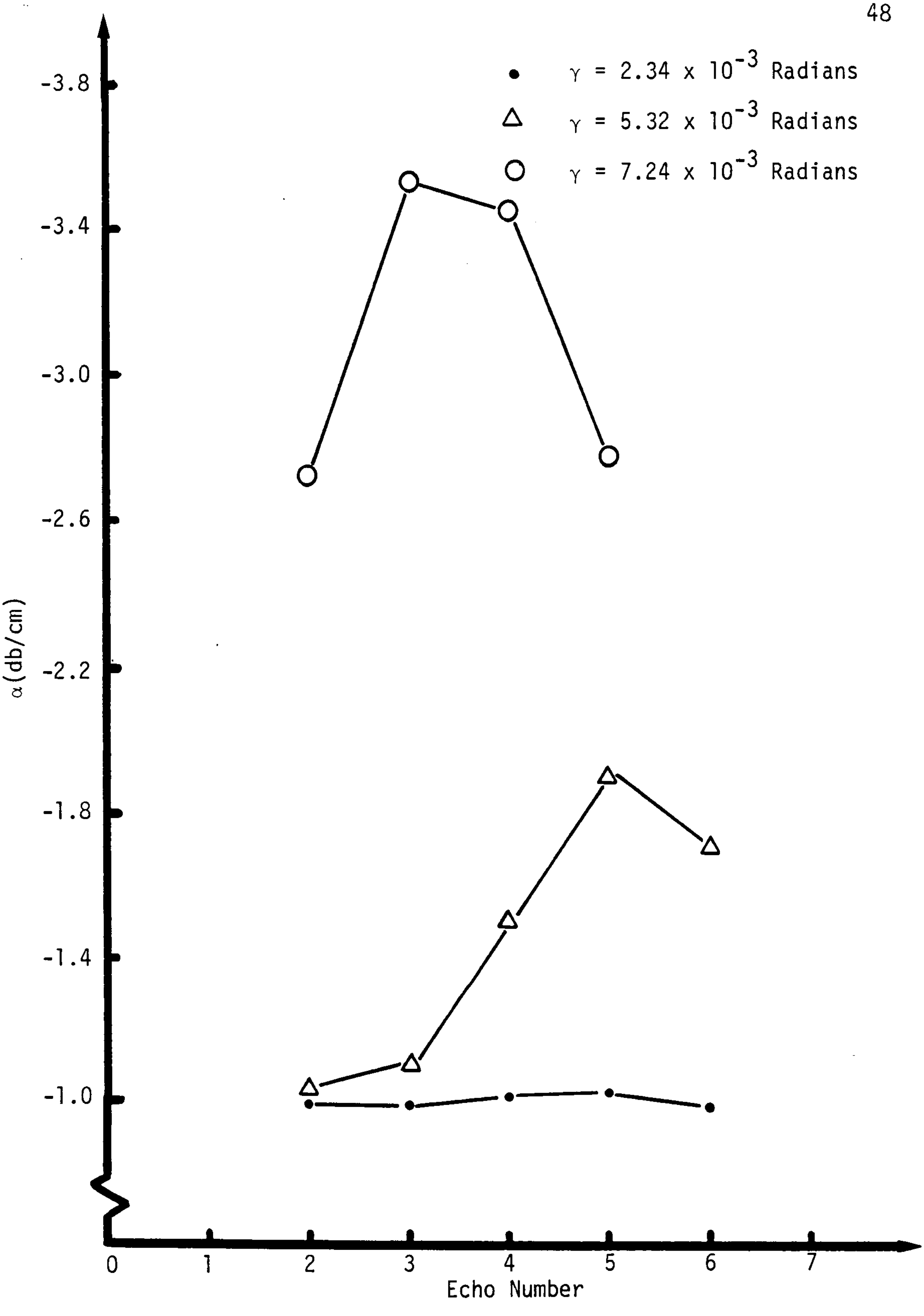

Figure IV-5. Apparent attenuation at 6 MHz for different wedge angles.

are given by the quantity DBDCA in the computer program in Appendix B. A plot of both the uncorrected and the diffraction corrected attenuation as a function of echo number is given in Figure IV-6. A reference attenuation obtained by taking the average of the attenuation values of the first four echoes also is plotted in this figure. From this plot one observes that the diffraction correction brings the first five echoes to within 5% of the reference attenuation. Furthermore, this reference attenuation value is deemed to represent the intrinsic attenuation for the steel under study as no comparative attenuation value for this material can be found in published literature. Beyond the fifth echo the correction overcompensates for the effects of diffraction. The deviation of the data from the reference attenuation for the latter part of the echo train may be attributable to two factors. First, the possibility exists that with increasing propagation distance the sound beam may be subjected to a wedge angle effect as reported by Boudreault (1982). The accuracy of our wedge angle measurements is limited to $\pm 3.0 \times 10^{-5}$ radians. If a wedge angle of 2×10^{-5} radians were present, then after four echoes the wave impinging on the receiver would approach it at the same wedge angle as the smallest wedge in the sample. Second, it is conceivable that one cannot neglect the uncertainty in measuring the small magnitudes of the higher order echoes. An estimate of this uncertainty for the seventh echo gave a value of ±36%, which is close to the magnitude of the correction of the seventh echo.

Having found that the model corrects the experimental data well in the range of large Ka values where the parabolic approximation should give good results, one now can examine the data taken for lower

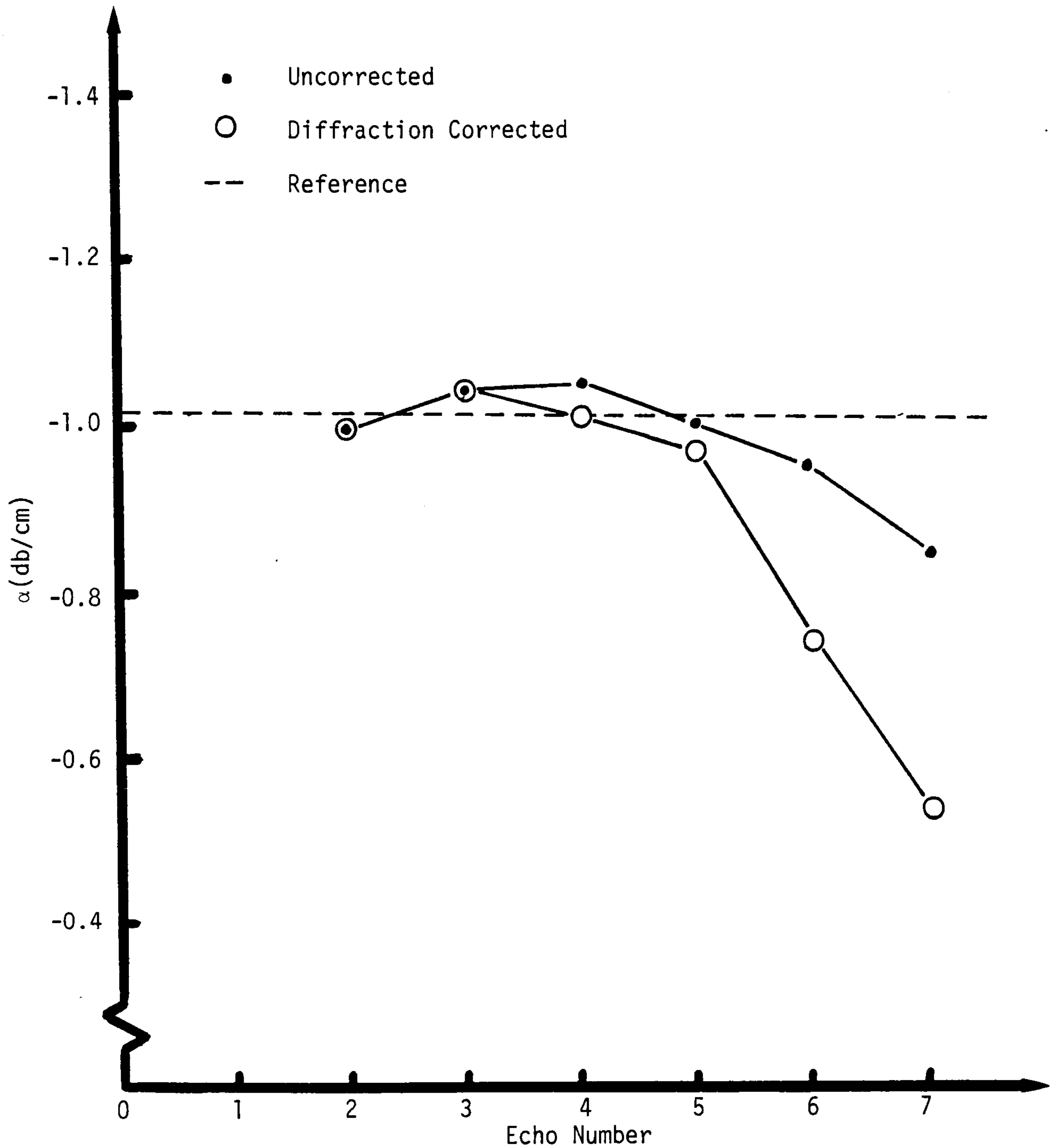

Figure IV-6. Attenuation at 6 MHz for 0 wedge angle. A reference attenuation is obtained by averaging the first four echoes.

Ka values. The diffraction correction applied to measurements taken at 3 MHz (Ka = 5) gave the results shown in Figure IV-7, in which it is clear that the model continues to adjust the attenuation for the first two echoes even at this low value of Ka. The reference attenuation shown in this figure is obtained by taking the average attenuation values of these two echoes.

In summary, one can use the model given in this study to correct the pressure measurements for diffraction for the first four echoes if Ka = 15. For Ka = 5 (2 or 3 MHz) the model seems to adjust the first two echoes properly. With this observation in mind, it now is possible to consider the effect of a change of the wedge angle.

C. Correction for Wedge Angle

It is evident from Figures IV-4 and IV-5 that the echo pattern and the measured attenuations are affected by the presence of a wedge angle. Using the geometrical correction defined by Equation (2-31) we now correct amplitude values obtained on facets with various wedge angles. A corrected attenuation is then obtained by using these corrected amplitude values in Equation (4-1). Again the attenuation is corrected by using the computer program in Appendix B to evaluate the quantity DBCGA. A plot of the corrected attenuation is then made against the echo number for several combinations of frequency and wedge angle. The reference level of attenuation determined from the average of the first few echo diffraction corrected attenuation values at zero wedge angle for each frequency again is plotted to serve as an

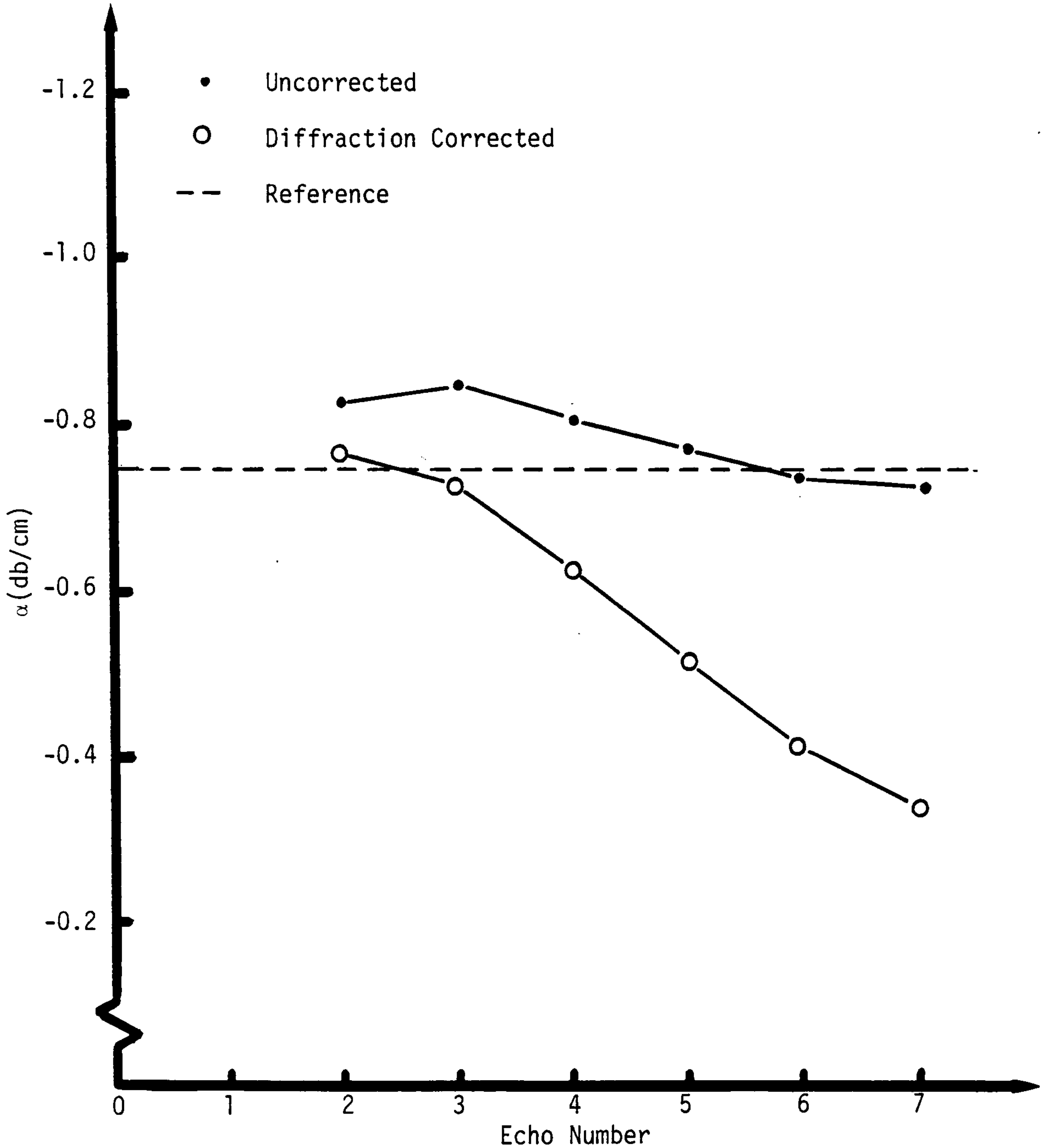

Figure IV-7. Attenuation at 3 MHz for 0 wedge angle. A reference attenuation is obtained by averaging the first two echoes.

indication of the degree of correction achieved at different wedge angles.

In Figure IV-8 is shown a plot of the data at 6 MHz for a wedge angle of 3.62×10^{-3} radians. This plot shows that the model properly adjusts the measured attenuation to within 10% of the reference level for the first four echoes. Since the model works this well, we now apply it to larger wedge angles and for lower frequencies. At large wedge angles, we observed that the geometrical correction adjusts the attenuation values in the right direction; however, it undercompensates for the variations produced by the wedge angle and diffraction. Representative plots illustrating this point are shown for 6 MHz in Figure IV-9 and for 3 MHz in Figure IV-10. In general, when the geometrical correction was applied to data at lower frequencies, we noted that the model was able to compensate for geometrical losses at specific combinations of frequency and wedge angle for at least the first few echoes. An example is shown in Figure IV-11 for a frequency of 3 MHz and wedge angle of 3.62×10^{-3} radians.

In summary, it is found that our geometrical model only corrects partially for the deviation of the measured attenuation from the reference at large wedge angles. For frequencies between 3 and 6 MHz and wedge angles less than 3.62×10^{-3} radians, the model adjusts the amplitude of the first few echoes to give good intrinsic attenuation values. In the data there appears to be an improvement in the correction for higher frequencies, so one might expect better and better results at higher and higher frequencies.

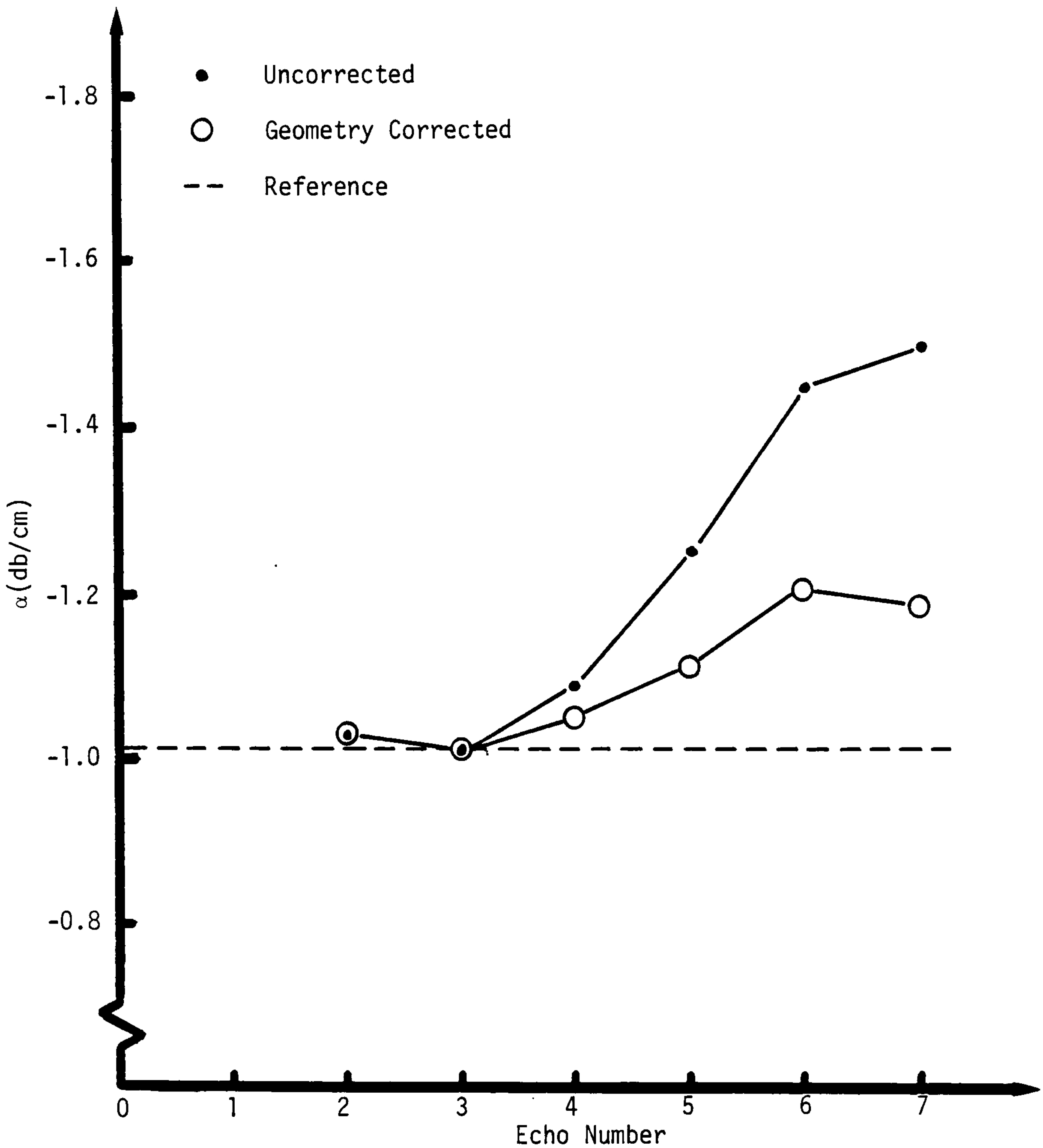

Figure IV-8. Attenuation at 6 MHz for a wedge angle of 3.62×10^{-3} radians using geometrical correction model and reference attenuation for $\gamma = 0$ and f = 6 MHz.

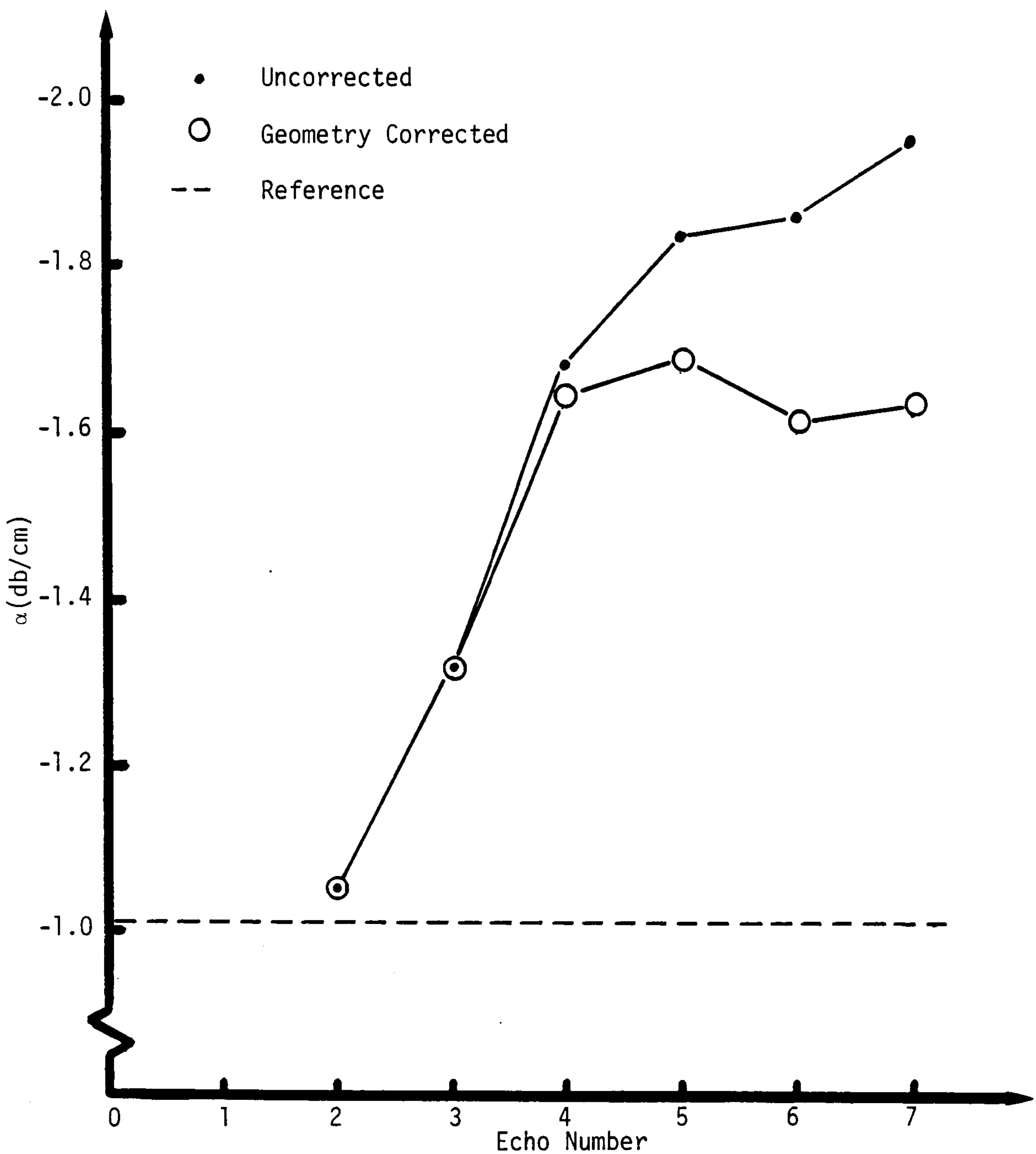

Figure IV-9. Attenuation at 6 MHz for a wedge angle of 7.24×10^{-3} radians using geometrical correction model and reference attenuation for $\gamma = 0$ and $f = 6$ MHz.

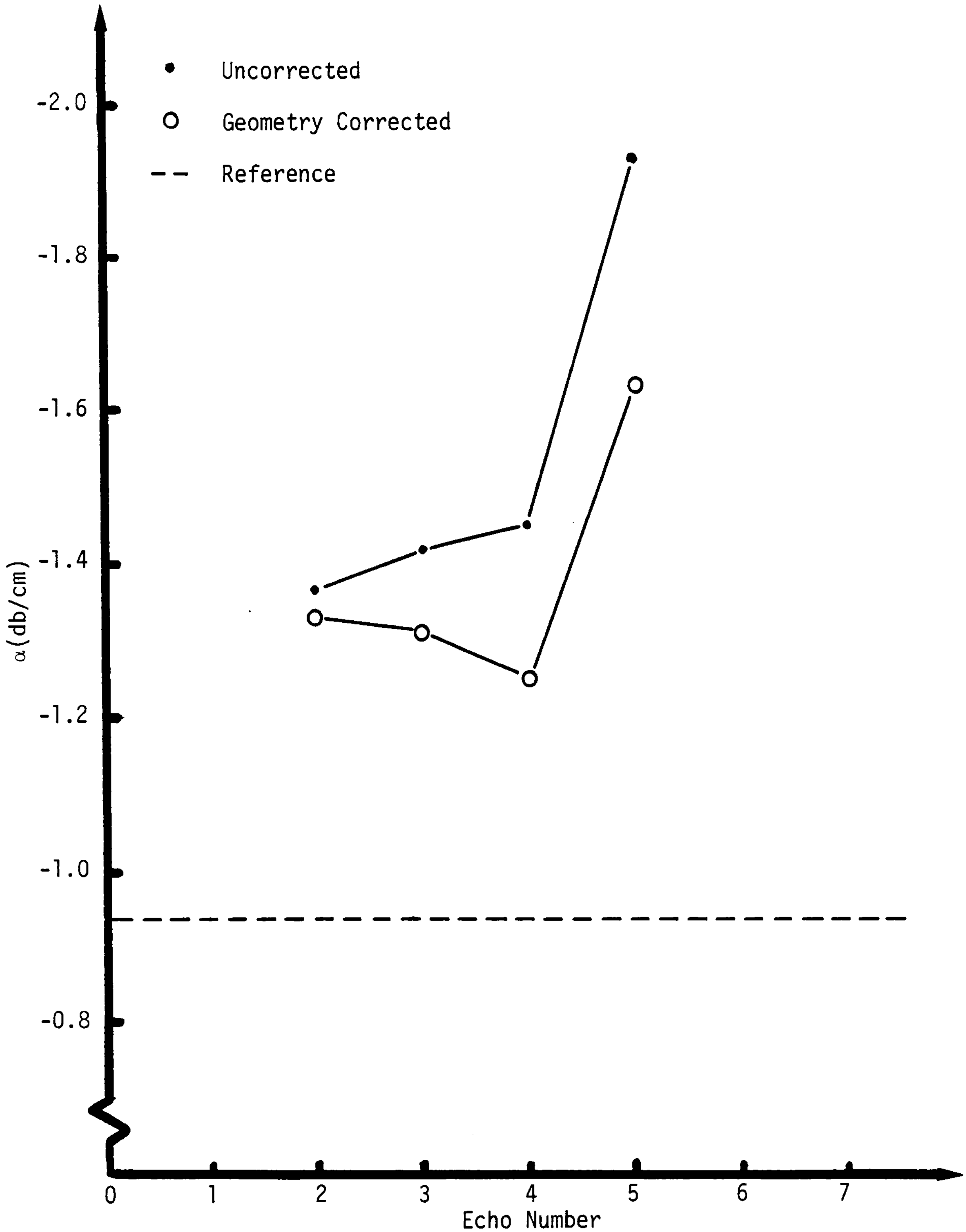

Figure IV-10. Attenuation at 3 MHz for a wedge angle of 9.51×10^{-3} radians using geometrical correction model and reference attenuation for $\gamma = 0$ and $f = 3$ MHz.

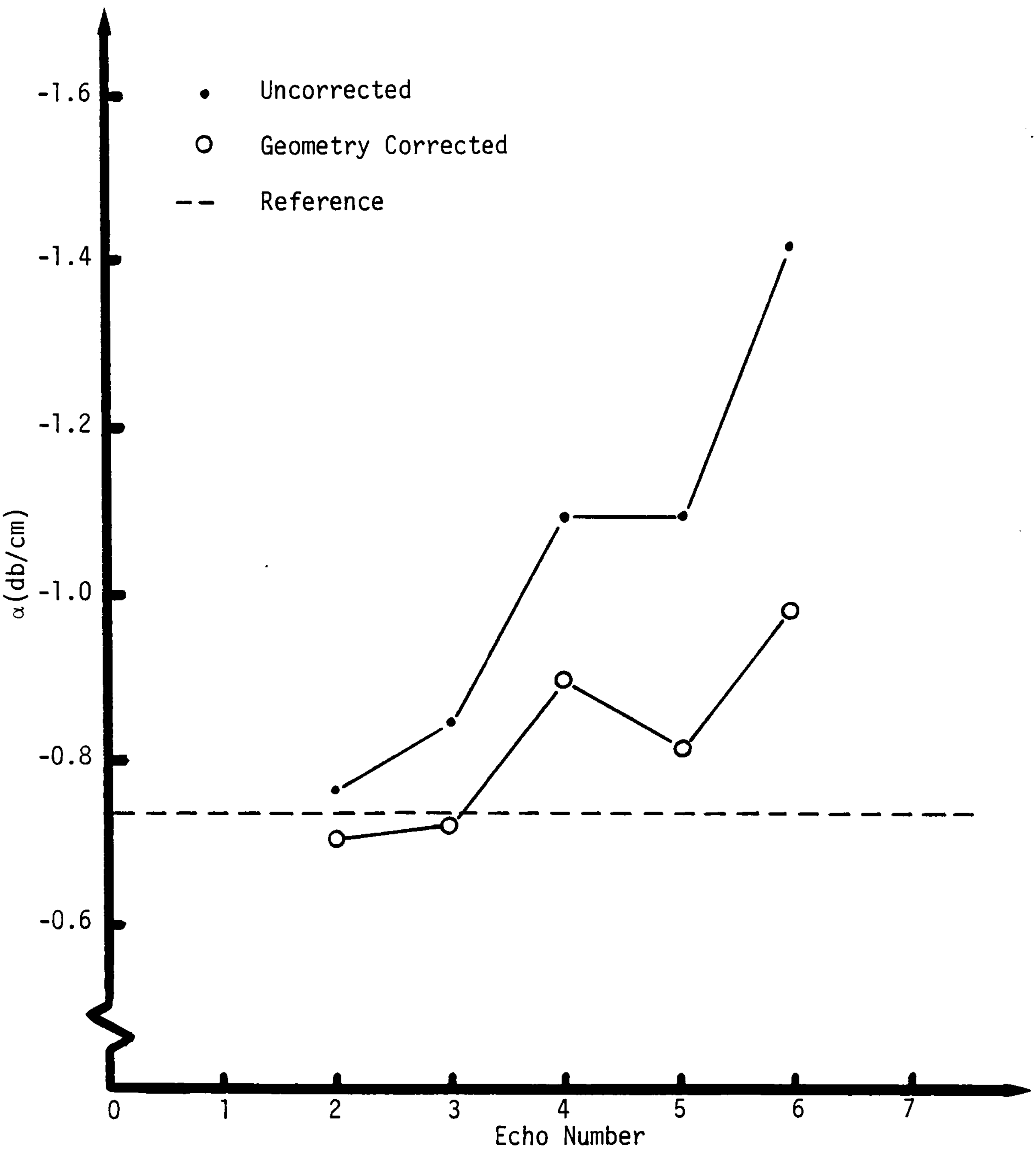

Figure IV-11. Attenuation at 3 MHz for wedge angle of 3.62 x 10^{-3} radians using geometrical correction model and reference attenuation for γ = 0 and f = 3 MHz.

D. Conclusion

An analytical theory for evaluating the effects of nonparallelism and diffraction on the measured pressure amplitude, and hence the attenuation, has been developed. This theory describes the ultrasonic field produced by a Gaussian transducer and is valid in the parabolic approximation. Using the corrections for diffraction and wedge angle as defined in the theory, corrections have been applied to data taken with a steel plate having wedge angles up to 1.81×10^{-2} radians. The diffraction correction at zero wedge angle seems to be valid at Ka values which satisfy the parabolic approximation (at Ka = 15) and for the first few echoes even at Ka values somewhat outside the limits of this approximation (at Ka = 5). Pressure amplitude corrections using the geometrical model for several combinations of frequency and wedge angle have provided good values for the first two echoes for all frequencies (2 to 6 MHz) and wedge angles less than 3.62×10^{-3} radians. This means that the model is able to make reasonably dependable adjustment of amplitude values in the range of frequencies commonly used in nondestructive testing. The only model previously available, that of Truell et al. (1969) corrects properly only for data taken at much higher frequencies (85 MHz). Further testing of the model is desirable, however, before it can be considered to be a reliable technique for field applications.

E. Suggestion for Further Study

From this investigation evolved a number of subjects which require further study.

1. A problem that was experienced in this study stemmed from a difficulty in exactly aligning the Gaussian transmitting transducer and receiving transducer. To overcome this problem it is felt that it would be beneficial to develop a single transducer that has the characteristics of the Gaussian in its transmit mode and provides a large receiving surface for returning echoes. This may be accomplished by depositing a doughnut shaped electrode on the outer part of the crystal and a small circular electrode in its center. By using suitable electronics one then could transmit a stress wave into the sample via the circular electrode in the center of the crystal and receive the returning echoes with the larger electrode on the outer part of the crystal.

2. A useful improvement of the diffraction model would be to extend its use to lower Ka values. This might be done by solving King's diffraction integral which is written in cylindrical coordinates for a Gaussian velocity distribution at the surface of the transducer.

LIST OF REFERENCES

LIST OF REFERENCES

Aanonsen, S. I., Barkve, T., Tjøtta, J. N., and Tjøtta, S., J. Acoust. Soc. Am. 75, 749 (1984).

Abramowitz, M. and Stegum, I. A., eds. Handbook of Mathematical Functions. Math. Ser. No. 55. Washington, D.C.: Government Printing Office, 1972.

Boudreault, J. P. S., "Effect of Nonparallelism on the Measurement of Ultrasonic Attenuation in Solids," Master's thesis, The University of Tennessee, Knoxville, 1982.

Breazeale, M. A., Martin, F. D., and Blackburn, B., J. Acoust. Soc. Am. 70, 1791 (1981).

Calder, I. D., J. Acoust. Soc. Am. 63, 967 (1978).

Du, G. and Breazeale, M. A., J. Acoust. Soc. Am. 76, S23 (A) (1984).

Filipczynski, L. and Etienne, J., Acustica 28, 121 (1973).

Greenspan, M., J. Acoust. Soc. Am. 65, 608 (1979).

Huntington, H. B., Emslie, A. G., and Hughes, V. M., J. Franklin Institute 245, 1 (1948).

Krautkrämer, J. and Haselberg, K. V., Acustica 9, 359 (1959).

Krautkrämer, J. and Krautkrämer, H., Ultrasonic Testing of Materials. Berlin/Heidelberg, Germany: Springer Verlay, 1977.

Lommel, E., Die Beugungserscheinungen einer Kreisrunden Oeffnung und eines Kreisnunder Schirmchens, Abhandl Math.-Phys. A. Konigl. Bayer. Akad. Wissensch 15, 2, 233 (1885).

Lord Rayleigh, The Theory of Sound, New York: Dover Publications, 1945, Vol. II.

Martin, F. D. and Breazeale, M. A., J. Acoust. Soc. Am. 49, 1668 (1971).

Palmer, C. H., Optics—Experiments and Demonstrations. Baltimore, Maryland: The John Hopkins Press, 1962.

Papadakis, E. P., Metall. Trans. 1, 1053 (1970).

Roderick, R. L. and Truell, R., J. Appl. Phys. 23, 267 (1952).

Rogers, E. H., "A Report Guide to Ultrasonic Attenuation Literature," AMRA-MS-65-09. Army Materials Research Agency, Watertown, Mass., 1965.

Rogers, P. H. and Van Buren, A. L., J. Acoust Soc. Am. 55, 724 (1974).

Scott, G. W., "Amplitude and Phase of Rayleigh-Angle Reflections of Gaussian Ultrasonic Beams Incident on Liquid-Solid Interfaces," Master's thesis, The University of Tennessee, Knoxville, 1975.

Seki, H., Granato, A., and Truell, R., J. Acoust. Soc. Am. 28, 230 (1956).

Sneddon, Ian N., Fourier Transforms. New York: McGraw-Hill Book Company, Inc., 1951.

Spiegel, M. R., Mathematical Handbook of Formula and Tables. New York: McGraw-Hill Book Company, Inc., 1968.

Truell, Rohn and Oates, W., J. Acoust. Soc. Am. 35, 1382 (1963).

Truell, Rohn, Elbaum, Charles, and Chick, Bruce B., Ultrasonic Methods in Solid State Physics. New York: Academic Press, 1969.

Vary, A., In Research Techniques in Nondestructive Testing (R. S. Sharpe, ed.), Vol. IV. London and New York: Academic Press, 1980.

Watson, G. N., A Treatise on the Theory of Bessel Functions. Cambridge, England: Cambridge University Press, 1944.

Zerwekh, P. S. and Claus, R. D., Proc. IEEE Ultrasonics Symposium, Vol. 2, 974 (1981).

APPENDICES

APPENDIX A

DESIGN OF A CIRCULAR GAUSSIAN TRANSDUCER

Du and Breazeale (1984) discussed a means by which one is able to produce a two-dimensional Gaussian amplitude distribution across a transducer by utilizing the effects of electrical fringing. The analytical basis for the design of a practical transducer derived from this study is presented as follows.

From electromagnetic theory, it is known that the electrical field produced by an element of a surface (Figure A-1) is given by:

$$dE = \frac{Q(t)}{\pi a^2} \rho d\rho d\theta \left(\frac{1}{R^2}\right) . \tag{A-1}$$

Here Q(t) represents the charge on the electrode, and a is the radius of the electrode.

The velocity amplitude at the surface of the transducer is assumed to be proportional to the z component of the electric field.

Thus, one writes:

$$dE_z = \frac{TQ(t)}{\pi a^2 R^3} \rho d\rho d\theta \tag{A-2}$$

where T is the thickness of the crystal.

The geometrical relationship $R^2 = r^2 + \rho^2 - 2r\rho\cos\phi\sin\theta$ is substituted into Equation (A-2) then integrated over the area of the electrode to obtain the electrical field at a point:

$$E_z = \frac{TQ(t)}{\pi a^2} \int_0^{2\pi} d\phi \int_0^a \frac{\rho d\rho}{(r^2 + \rho^2 - 2r\rho\cos\phi\sin\theta)^{3/2}} . \tag{A-3}$$

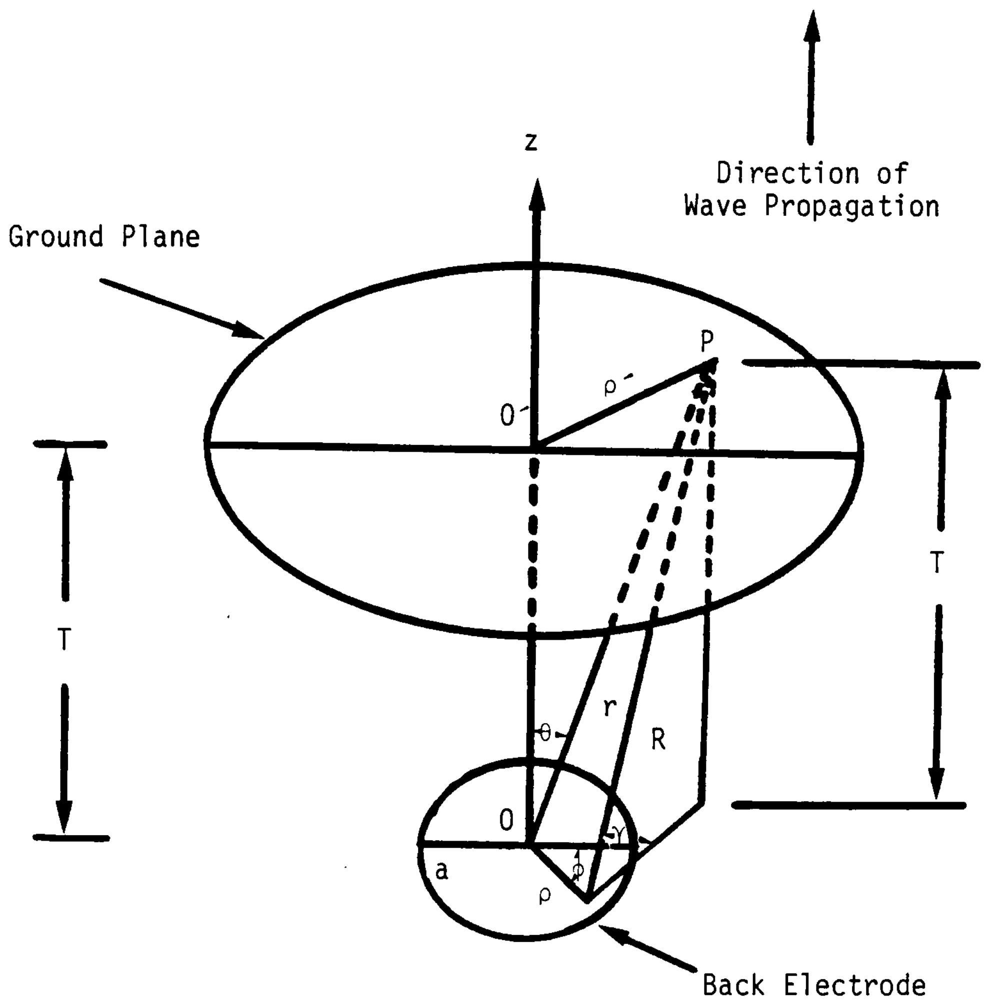

Figure A-1. Coordinates for calculating the electrical field.

Source: G. Du and M. A. Breazeale, J. Acoust. Soc. Am. 76, S23 (A) (1984).

Integrating Equation (A-3) with respect to ρ by changing the variable of integration to $\omega = r/\rho$ one gets:

$$E_z = \frac{TQ(t)}{\pi a^2} \int_0^{2\pi} d\phi \, \frac{1}{r} \int_0^{a/r} \frac{\omega d\omega}{(\omega^2 - 2\omega\cos\phi\sin\theta + 1)^{3/2}} \, . \qquad \text{(A-4)}$$

From Spiegel (1968):

$$\int \frac{xdx}{(Ax^2 + Bx + C)^{3/2}} = \frac{2(Bx + 2C)}{(B^2 - 4AC)(Ax^2 + Bx + C)^{1/2}} \, .$$

Thus, Equation (A-4) becomes:

$$E_z = \frac{2TQ(t)}{\pi a^2 r} \left(\int_0^{2\pi} \frac{(1 - \frac{a}{r}\sin\theta\cos\phi)d\phi}{(1 - \sin^2\theta\cos^2\phi)(\frac{a^2}{r^2} - 2(\frac{a}{r})\sin\theta\cos\theta + 1)^{1/2}} \right.$$

$$\left. - \int_0^{2\pi} \frac{d\phi}{1 - \sin^2\theta\cos^2\theta} \right) \, . \qquad \text{(A-5)}$$

One may evaluate the second integral of Equation (A-5) by using Spiegel (1968),

$$\int \frac{dx}{p^2 - q^2\cos^2 Ax} = \frac{1}{Ap^2(p^2 - q^2)^{1/2}} \tan^{-1} \left(\frac{p \tan(Ax)}{(p^2 - q^2)^{1/2}} \right) \, , \qquad \text{(A-6)}$$

to get:

$$E_z = \frac{TQ(t)}{\pi a^2 r} \left(\frac{-2\pi}{\cos\theta} + \int_0^{2\pi} \frac{(1 - \frac{a}{r}\sin\theta\cos\phi)d\phi}{(1 - \sin^2\theta\cos^2\phi)\left(\frac{a^2}{r^2} - 2(\frac{a}{r})\cos\phi\sin\theta + 1\right)^{1/2}} \right) . \qquad \text{(A-7)}$$

Recalling the geometric relationships $\cos\theta = \frac{T}{r}$ and $\sin\theta = \frac{\rho'}{r}$ from Figure A-1 one may rewrite Equation (A-7) to get:

$$E_z = -\frac{2Q(t)}{a^2} + \frac{TQ(t)}{\pi a^2 r}\int_0^{2\pi} \frac{(1 - \frac{a\rho'}{r^2}\cos\phi)d\phi}{(1 - \frac{\rho'^2}{r^2}\cos^2\phi)((\frac{a}{r})^2 - 2(\frac{a\rho'}{r^2})\cos\phi + 1)^{1/2}} .$$

(A-8)

Simplifying Equation (A-8) one gets:

$$E_z = \frac{2Q(t)}{a^2}\left[-1 + \frac{1}{\pi}\int_0^{2\pi} \frac{T(\eta - \varepsilon\cos\phi)d\phi}{(\eta - \varepsilon^2\cos^2\phi)(1 - 2\varepsilon\cos\phi + \eta)^{1/2}}\right] \quad \text{(A-9)}$$

where $\varepsilon = \frac{\rho'}{a}$ and $\eta = (\frac{r}{a})^2$.

Now one may normalize and numerically integrate Equation (A-9) to get a plot of the electrical field across the surface of a transducer and hence the velocity amplitude distribution. Results of such an integration for a D/T ratio of three are shown in Figure A-2. For comparison, the curve representing a Gaussian distribution with a coefficient B = 0.4861 is also shown. This value of Gaussian coefficient is used in the calculations presented in this study.

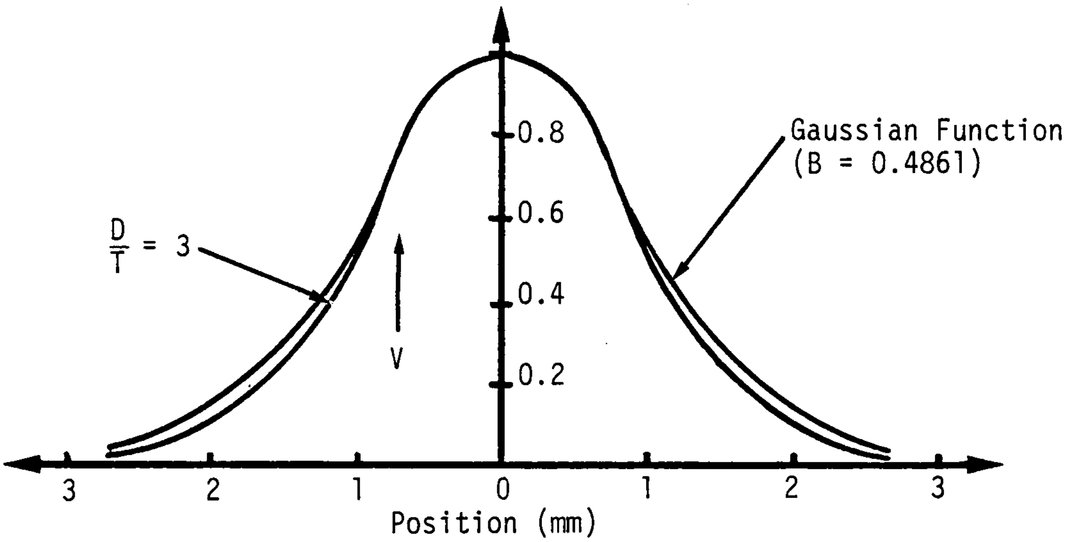

Figure A-2. Comparison of the electric field for a D/T = 3 and Gaussian function.

Source: G. Du and M. A. Breazeale, J. Acoust. Soc. Am. 76, S23 (A) (1984).

APPENDIX B

A COMPUTER PROGRAM FOR CORRECTING ATTENUATION DATA

```
10    REM THIS PROGRAM IS CODED IN IBM PERSONNAL
20    REM COMPUTER BASIC LANGUAGE. IT CALCULATES
30    REM THE CORRECTED ATTENUATION BETWEEN ECHO 1
40    REM AND NN (NN<10) FOR THE THROUGH-
50    REM TRANSMISSION TESTING TECHNIQUE.
60    REM
70    REM
80    REM THE INPUT VARIABLES ARE:
90    REM         NN          : NUMBER OF ECHOES
100   REM         DAT(NN,2):  UNCORRECTED AMPLITUDE
110   REM                       MEASUREMENTS (VOLTS)
120   REM         BG          : GAUSSIAN COFFICIENT
130   REM         CO          : VELOCITY OF THE ULTRASONIC
140   REM                       WAVE IN THE SAMPLE (M/SEC)
150   REM         F4          : FREQUENCY (HZ)
160   REM         WA          : WEDGE ANGLE (DEGREES)
170   REM         TS          : SAMPLE THICKNESS (M)
180   REM         A6          : RADIUS OF THE GAUSSIAN
190   REM                       ELECTRODE (M)
200   REM         A8          : RADIUS OF THE RECEIVING
210   REM                       TRANSDUCER (M)
220   REM
230   REM
240   REM THE OUTPUT VARIABLES ARE:
250   REM         DBXXX       : ATTENUATION (DB/CM)
260   REM         WHERE XXX STANDS FOR:
270   REM                 DBUC   : UNCORRECTED
280   REM                          ATTENUATION
290   REM                 DBDCA  : CORRECTED FOR
300   REM                          DIFFRACTION
310   REM                 DBCGA  : CORRECTED FOR
320   REM                          DIFFRACTED WAVE
330   REM                          GEOMETRY
340   REM
350   REM
360   DEFDBL A-H,P-Z
370   DEFINT I-O
380   DIM U(16),W(16),V(15),Z(15),A(2)
390   DIM DAT(10,4),PR(10,3),DBB(10),DBX(10)
400   AX$="##        ##.##      ##.##"
410   INPUT "NO OF ECHOES";NN
```

```
420  REM
430  REM READ IN THE DATA FOR THE GAUSSIAN QUADRATURE
440  REM
450  FOR I=1 TO 15
460  READ U(I),W(I),V(I),Z(I)
470  NEXT I
480  READ U(16),W(16)
490  REM
500  REM READ IN THE UNCORRECTED ATTENUATION MEASUREMENTS
510  REM
520  FOR I=1 TO NN
530  INPUT "UNCORRECTED AMPLITUDE VALUE (VOLTS)"; DAT(I,2)
540  NEXT I
550  FOR IX= 2 TO NN
560  WX=DAT(IX,2)/DAT(1,2)
570  DBB(IX)=.4342944819#*20#*LOG(WX)
580  NEXT IX
590  REM
600  REM INPUT THE DATA PARMETERS FOR THE EXPERIMENT
610  REM
620  INPUT "BG (GAUSSIAN COEFF)";BG
630  INPUT "WA (DEGREES)";WA
640  INPUT "CO (M/SEC)";CO
650  INPUT "F4 (HZ)";F4
660  INPUT "TS (M)";TS
670  INPUT "A6 (M)";A6
680  INPUT "A8 (M)";A8
690  PRINT
700  PRINT
710  CLS
720  PI=3.14159265358979#
730  A(1)=0:A(2)=A8/A6
740  REM
750  REM BEGIN LOOP FOR THE INTEGRATION
760  REM
770  FOR J=1 TO 2
780  A2=A(J)
790  REM
800  REM BEGIN LOOP FOR CORRECTION OF THE ECHOES
810  REM
820  FOR N=1 TO NN STEP 1
830  RAD=WA*PI/180#
840  AN=(2*N-1)*RAD
850  SL=TS*CO/((A6^2)*PI*F4)
860  S1=(2*N-1)*SL
870  W1=SIN(AN)
880  E2=BG/(1+(BG*S1)^2)
```

```
890  A1=1/((1+(BG*S1)^2)^.5)
900  GOSUB 1670
910  GOSUB 2100
920  PRE=A1*((C2^2)+(C4^2))^.5
930  PR(N,1)=PRE
940  IF NOT(A2=0) THEN 960
950  SWAP PR(N,1),PR(N,2)
960  NEXT N
970  NEXT J
980  FOR JJ=1 TO NN STEP 1
990  PR(JJ,3)=PR(JJ,2)-PR(JJ,1)
1000  NEXT JJ
1010  FOR NX=2 TO NN STEP 1
1020  WW=PR(NX,3)/PR(1,3)
1030  DB=.434294481903#*20#*LOG(WW)
1040  DAT(NX-1,4)=(DBB(NX)-DB)/((NX*2-2)*TS*100)
1050  DBX(NX)=DBB(NX)/((NX*2-2)*TS*100)
1060  NEXT NX
1070  REM
1080  REM PRINT OUT EXPERIMENTAL PARMETERS
1090  REM
1100  PRINT"BG=" BG  "(GAUSSIAN COEFF)"
1110  PRINT"CO=" CO "(M/SEC)"
1120  PRINT"F4=" F4 "(HZ)"
1130  PRINT"TS=" TS "(M)"
1140  PRINT"A6=" A6 "(M)"
1150  PRINT"NN=" NN "(NO OF ECHOES)"
1160  PRINT"WA=" WA "(DEGREES)"
1170  PRINT
1180  PRINT
1190  PRINT
1200  REM
1210  REM PRINT OUT THE RESULTS
1220  REM
1230  PRINT "THE RESULTS ARE:"
1240  PRINT
1250  IF WA=0 THEN PRINT "ECHO       DBUC       DBDCA"
1260  IF WA<0 THEN PRINT "ECHO       DBUC       DBCGA"
1270  PRINT
1280  FOR I=1 TO NN-1
1290  PRINT USING AX$;I+1;DBX(I+1);DAT(I,4)
1300  NEXT I
1310  END
1320  REM
1330  REM DATA BLOCK FOR GAUSSIAN QUADRATURE
1340  REM
1350  DATA .04830766568773832,.09654008851472780
```

```
1360  DATA .093307812017,.239578170311
1370  DATA .1444719615827964 9,.0956387200792748 6
1380  DATA .492691740302,.560100842793
1390  DATA .2392873622521370 7,.0938443990808045 7
1400  DATA 1.215595412071,.887008262919
1410  DATA .3318686022821276 5,.0911738786957638 8
1420  DATA 2.269949526204,1.22366440215
1430  DATA .4213512761306353 5,.0876520930044038 1
1440  DATA 3.667622721751,1.57444872163
1450  DATA .5068999089322293 9,.0833119242269467 6
1460  DATA 5.425336627414,1.94475197653
1470  DATA .5877157572407623 3,.0781938957870703 1
1480  DATA 7.565916226613,2.34150205664
1490  DATA .6630442669302152 0,.0723457941088485 1
1500  DATA 10.120228568019,2.77404192683
1510  DATA .7321821187402896 8,.0658222227763618 5
1520  DATA 13.130282482176,3.25564334640
1530  DATA .7944837959679424 1,.0586840934785355 5
1540  DATA 16.654407708330,3.80631171423
1550  DATA .8493676137325699 7,.0509980592623761 8
1560  DATA 20.776478899449,4.45847775384
1570  DATA .8963211557660521 2,.0428358980222266 8
1580  DATA 25.623894226729,5.27001778443
1590  DATA .9349060759377396 9,.0342738629130214 3
1600  DATA 31.407519169754,6.35956346973
1610  DATA .9647622555875064 3,.0253920653092620 6
1620  DATA 38.530683306486,8.03178763212
1630  DATA .9856115115452683 4,.0162743947309056 7
1640  DATA 48.026085572686,11.5277721009
1650  DATA .9972638618494815 6,.0070186100094701 0
1660  REM
1670 REM GAUSSIAN QUADRATURE
1680 P=.0001
1690 B=300
1700 M=1
1710 H=(B-A2)/M
1720 H2=H/2!
1730 C1=0!
1740 C2=0!
1750 C3=A2-H2
1760 FOR JJ=1 TO M
1770 D1=H*JJ
1780 FOR I=1 TO 16
1790 X=H2*U(I)
1800 X5=C3+D1+X
1810 X6=C3+D1-X
1820  FA1=X5*EXP(-E2*(X5^2))*SIN(-ATN(BG*(S1-X5*W1))
+(((BG^2)*(S1-X5*W1))*X5^2/(1+(BG*(S1-X5*W1))^2)))
```

```
1830  FA2=X6*EXP(-E2*(X6^2))*SIN(-ATN(BG*(S1-X6*W1))
+(((BG^2)*(S1-X6*W1))*X6^2/(1+(BG*(S1-X6*W1))^2)))
1840 C2=C2+W(I)*(FA1+FA2)
1850 NEXT I
1860 NEXT JJ
1870 C2=C2*H2
1880 IF P=0 THEN GOTO 2010
1890 IF C1=4 THEN GOTO 2000
1900 REM TESTING ACCURACY OF INTERGRATION
1910 IF C1=0 THEN GOTO 1940
1920 D9=ABS((C2-C8)/C2)
1930 IF D9<P THEN GOTO 2000
1940 C8=C2
1950 C1=C1+1
1960 M=M+M
1970 H=H2
1980 H2=H2/2
1990 GOTO 1740
2000 REM LAGUERRE QUADRATURE
2010 C22=C2
2020 C2=0
2030 FOR I = 1 TO 15
2040 X=B+V(I)
2050  F2=X*EXP(-E2*(X^2))*SIN(-ATN(BG*(S1-X*W1))
+(((BG^2)*(S1-X*W1))*X^2/(1+(BG*(S1-X*W1))^2)))
2060 C2=C2+Z(I)*F2
2070 NEXT I
2080 C2=C2+C22
2090 RETURN
2100 REM GAUSSIAN QUADRATURE
2110 P=.0001
2120 B=300
2130 M=1
2140 H=(B-A2)/M
2150 H2=H/2!
2160 C1=0!
2170 C4=0!
2180 C3=A2-H2
2190 FOR JJ = 1 TO M
2200 D1=H*JJ
2210 FOR I = 1 TO 16
2220 X=H2*U(I)
2230 X5=C3+D1+X
2240 X6=C3+D1-X
2250  GA1=X5*EXP(-E2*(X5^2))*COS(-ATN(BG*(S1-X5*W1))
+(((BG^2)*(S1-X5*W1))*X5^2/(1+(BG*(S1-X5*W1))^2)))
2260  GA2=X6*EXP(-E2*(X6^2))*COS(-ATN(BG*(S1-X6*W1))
+(((BG^2)*(S1-X6*W1))*X6^2/(1+(BG*(S1-X6*W1))^2)))
```

```
2270 C4=C4+W(I)*(GA1+GA2)
2280 NEXT I
2290 NEXT JJ
2300 C4=C4*H2
2310 IF P=0 THEN GOTO 2440
2320 IF C1=4 THEN GOTO 2430
2330 REM TESTING ACCURACY OF INTERGRATION
2340 IF C1=0 THEN GOTO 2370
2350 D9=ABS((C4-C8)/C4)
2360 IF D9<P THEN GOTO 2430
2370 C8=C4
2380 C1=C1+1
2390 M=M+M
2400 H=H2
2410 H2=H2/2
2420 GOTO 2170
2430 REM LAGUERRE QUADRATURE
2440 C44=C4
2450 C4=0
2460 FOR I = 1 TO 15
2470 X=B+V(I)
2480  F3=X*EXP(-E2*(X^2))*COS(-ATN(BG*(S1-X*W1))
+(((BG^2)*(S1-X*W1))*X^2/(1+(BG*(S1-X*W1))^2)))
2490 C2=C2+Z(I)*F3
2500 NEXT I
2510 C4=C4+C44
2520 RETURN
```

VITA

Edward Ted Karkut was born in Woodstock, Ontario, Canada, on August 19, 1956. He attended public schools in that city and graduated from Huron Park Secondary School in June 1975. In August he joined the Canadian Armed Forces under the Regular Officer Training Program and commenced his university education at the Royal Military College in Kingston, Ontario. He received his Bachelor of Engineering in Mechanical Engineering from that institution in May 1979.

After a three-year tour of duty at Moose Jaw, Saskatchewan as an Aerospace Engineering Officer he was selected to attend Graduate School under the sponsorship of the Canadian Forces Post Graduate Training Program. Subsequently he entered the Graduate School of The University of Tennessee, Knoxville, in September 1983.

He was married to the former Mary Katherine O'Neill of Gananoque, Ontario on October 6, 1979. They have no children.